JHEP02(2017)135

Searches for invisible decays of the Higgs boson in pp collisions at $\sqrt{s} = 7$, 8, and 13 TeV

The CMS collaboration

E-mail: cms-publication-committee-chair@cern.ch

ABSTRACT: Searches for invisible decays of the Higgs boson are presented. The data collected with the CMS detector at the LHC correspond to integrated luminosities of 5.1, 19.7, and 2.3 fb^{-1} at centre-of-mass energies of 7, 8, and 13 TeV, respectively. The search channels target Higgs boson production via gluon fusion, vector boson fusion, and in association with a vector boson. Upper limits are placed on the branching fraction of the Higgs boson decay to invisible particles, as a function of the assumed production cross sections. The combination of all channels, assuming standard model production, yields an observed (expected) upper limit on the invisible branching fraction of 0.24 (0.23) at the 95% confidence level. The results are also interpreted in the context of Higgs-portal dark matter models.

Contents

1 Introduction

The Higgs boson (H) discovery and the study of its properties by the ATLAS and CMS Collaborations [1–3] at the CERN LHC have placed major constraints on potential models of new physics beyond the standard model (SM). Precision measurements of the couplings of the Higgs boson from a combination of the 7 and 8 TeV ATLAS and CMS data sets indicate a very good agreement between the measured properties of the Higgs boson and the SM predictions [4]. In particular, these measurements provide indirect constraints on additional contributions to the Higgs boson width from non-SM decay processes. The

resulting indirect upper limit on the Higgs boson branching fraction to non-SM decays is 0.34 at the 95% confidence level (CL) [4].

A number of models for physics beyond the SM allow for invisible decay modes of the Higgs boson, such as decays to neutralinos in supersymmetric models [5] or graviscalars in models with extra spatial dimensions [6, 7]. More generally, invisible Higgs boson decays can be realised through interactions between the Higgs boson and dark matter (DM) [8]. In Higgs-portal models [9–12], the Higgs boson acts as a mediator between SM and DM particles allowing for direct production of DM at the LHC. Furthermore, cosmological models proposing that the Higgs boson played a central role in the evolution of the early universe motivate the study of the relationship between the Higgs boson and DM [13, 14].

Direct searches for invisible decays of the Higgs boson increase the sensitivity to the invisible Higgs boson width beyond the indirect constraints. The typical signature at the LHC is a large missing transverse momentum recoiling against a distinctive visible system. Previous searches by the ATLAS and CMS Collaborations have targeted Higgs boson production in association with a vector boson (VH, where V denotes W or Z) [15–17] or with jets consistent with a vector boson fusion (VBF, via qq → qqH) topology [17, 18]. A combination of direct searches for invisible Higgs boson decays in qqH and VH production, by the ATLAS Collaboration, yields an upper limit of 0.25 on the Higgs boson invisible branching fraction, $\mathcal{B}(H \to inv)$, at the 95% confidence level [19]. Additionally, searches by the ATLAS Collaboration for DM in events with missing transverse momentum accompanied by jets have been interpreted in the context of Higgs boson production via gluon fusion and subsequent decay to invisible particles [20].

In this paper, results from a combination of searches for invisible decays of the Higgs boson using data collected during 2011, 2012, and 2015 are presented. The searches target the qqH, VH, and ggH production modes. The searches for the VH production mode include searches targeting ZH production, in which the Z boson decays to a pair of leptons (either e^+e^- or $\mu^+\mu^-$) or $b\overline{b}$, and searches for both the ZH and WH production modes, in which the W or Z boson decays to light-flavour jets. Additional sensitivity is achieved in this analysis by including a search targeting gluon fusion production where the Higgs boson is produced accompanied by a gluon jet (gg → gH). The diagrams for the qqH, VH, and ggH Higgs boson production processes are shown in figure 1. The contribution to ZH production from gluon fusion (gg → ZH), as shown in figure 2, is included in this analysis. When combining the searches to determine an upper limit on $\mathcal{B}(H \to inv)$ SM production cross sections are assumed, consistent with the measured Higgs boson production rates [4]. In addition, upper limits on $\mathcal{B}(H \to inv)$ assuming non-SM production cross sections are provided.

This paper is structured as follows: a brief overview of the CMS detector and event reconstruction is given in section 2, and the data sets and simulation used for the searches are presented in section 3. In section 4, the strategy for each search included in the combination is described, and in section 5 the results of the searches are presented and interpreted in terms of upper limits on $\mathcal{B}(H \to inv)$ and DM-nucleon interaction cross sections. Finally, a summary is presented in section 6.
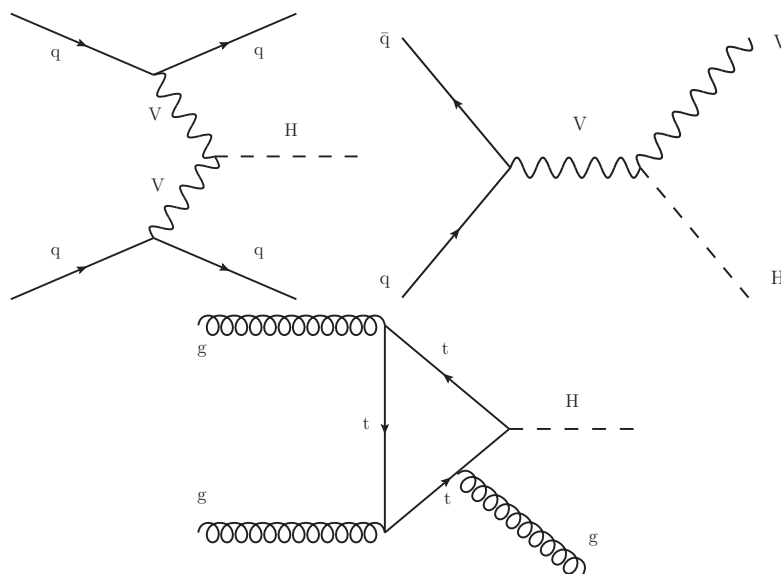
Figure 1. Feynman diagrams for the three production processes targeted in the search for invisible Higgs boson decays: (upper left) qq → qqH, (upper right) q$\bar{\text{q}}$ → VH, and (bottom) gg → gH.
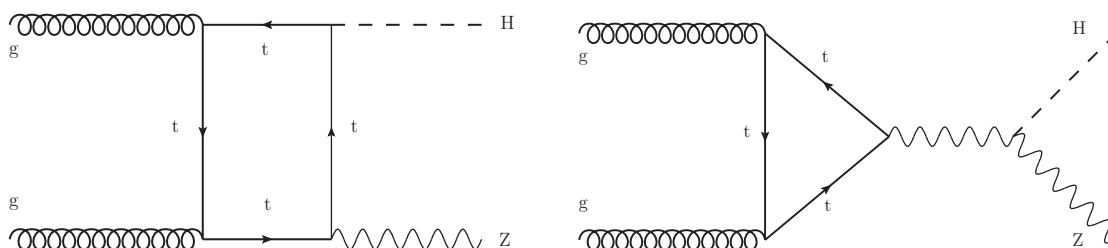

Figure 2. Feynman diagrams for the gg→ZH production processes involving a coupling between (left) the top quark and the Higgs boson or (right) the Z and Higgs bosons.

2 The CMS detector and object reconstruction

The CMS detector is a multipurpose apparatus optimised to study high transverse momentum (p_{T}) physics processes in proton-proton and heavy-ion collisions. A superconducting solenoid occupies its central region, providing a magnetic field of 3.8 T parallel to the beam direction. Charged-particle trajectories are measured by the silicon pixel and strip trackers, which cover a pseudorapidity region of $|\eta| < 2.5$. A lead tungstate crystal electromagnetic calorimeter (ECAL), and a brass and scintillator hadron calorimeter (HCAL) surround the tracking volume and cover $|\eta| < 3$. The steel and quartz-fibre Cherenkov hadron forward calorimeter extends the coverage to $|\eta| < 5$. The muon system consists of gas-ionisation detectors embedded in the steel flux-return yoke outside the solenoid, and covers $|\eta| < 2.4$. The first level of the CMS trigger system, composed of custom hardware processors, is designed to select the most interesting events in less than $4\,\mu$s, using information from the calorimeters and muon detectors. The high-level trigger processor farm then further reduces the event rate to less than $1\,$kHz. A more detailed description of the CMS detec-

tor, together with a definition of the coordinate system used and the relevant kinematic variables, can be found in ref. [21].

Objects are reconstructed using the CMS particle-flow (PF) algorithm [22, 23], which optimally combines information from the various detector components to reconstruct and identify individual particles. The interaction vertex with the maximum value of $\sum_i (p_T^i)^2$, where p_T^i is the transverse momentum of the ith track associated with the vertex, is selected as the primary vertex for the reconstruction of these objects.

Jets are reconstructed by clustering PF candidates, using the anti-k_T algorithm [24] with a distance parameter of 0.5 (0.4) for the 7 and 8 (13) TeV data set. Analyses exploring Lorentz-boosted hadronic objects employ large-radius jets, clustered using the Cambridge-Aachen algorithm [25] at 8 TeV and the anti-k_T algorithm at 13 TeV, each with a distance parameter of 0.8. The combined secondary vertex algorithm is used to identify jets originating from b quarks (b jets) [26–28]. The selection used is roughly 70% efficient for b jets with $p_T > 30$ GeV.

The jet momentum is corrected to account for contamination from additional interactions in the same bunch crossing (pileup, PU) based on the event energy density scaled proportionally to the jet area [29]. Calibrations based on simulation and control samples in data are applied to correct the absolute scale of the jet energy [30]. The jets are further subjected to a standard set of identification criteria [31]. All jets are required to have $p_T > 30$ GeV and $|\eta| < 4.7$, unless stated otherwise.

The missing transverse momentum vector $\vec{p}_T^{\text{miss}}$ is defined as the projection on the plane perpendicular to the beams of the negative vector sum of the momenta of all PF candidates in the event. The magnitude of $\vec{p}_T^{\text{miss}}$ is referred to as E_T^{miss}. Dedicated quality filters are applied for tracks, muons, and other physics objects to remove events with large misreconstructed E_T^{miss}.

Electron (e), photon (γ), and muon (μ) candidates are required to be within the relevant detector acceptances of $|\eta| < 2.5$ (e/γ) and $|\eta| < 2.4$ (μ). Electron and photon candidates in the transition region between the ECAL barrel and endcap ($1.44 < |\eta| < 1.57$) are not considered because the reconstruction of electrons and photons in this region is not optimal. Details of the electron, photon, and muon reconstruction algorithms and their performance can be found in refs. [32, 33], and [34], respectively.

Lepton isolation is based on the sum of the p_T of additional PF candidates in a cone of radius $R = \sqrt{(\Delta\eta)^2 + (\Delta\phi)^2} = 0.4$ around each lepton, where $\Delta\phi$ and $\Delta\eta$ are the differences in azimuthal angle (in radians) and pseudorapidity between the lepton and each particle in the sum, respectively. The isolation sum is required to be smaller than 15% (12%) of the electron (muon) p_T. In order to reduce the dependence of the isolation variable on the number of PU interactions, charged hadrons are included in the sum only if they are consistent with originating from the selected primary vertex of the event. To further correct for the contribution of neutral particles from PU events to the isolation sum in the case of electrons, the median transverse energy density, determined on an event-by-event basis as described in ref. [35], is subtracted from the sum. For muons the correction is made by subtracting half the sum of the transverse momenta of charged particles that are inside the cone and not associated with the primary vertex. The factor of one half

accounts for the expectation that there are half the number of neutral particles as charged particles within the cone.

Details of the reconstruction of τ leptons can be found in ref. [36]. The sum of the transverse momenta of all PF candidates within a cone of radius $\Delta R < 0.3$ around the τ candidates is required to be less than $5\,\mathrm{GeV}$.

For the purposes of event vetoes, a set of electron, photon, muon, and τ-lepton identification and isolation criteria are applied as defined by the "loose" selections in refs. [32, 33, 37], and [36], respectively. To veto an event the electron, photon, or muon must have $p_\mathrm{T} > 10\,\mathrm{GeV}$ and fall within the detector acceptance described above, while a τ-lepton must have $p_\mathrm{T} > 15\,\mathrm{GeV}$ and $|\eta| < 2.3$. These vetoes suppress backgrounds from leptonic decays of electroweak (EW) backgrounds and allow orthogonal control regions.

3   Data samples and simulation

The data used for the analyses described here comprise pp collisions collected with the CMS detector in the 2011, 2012, and 2015 data-taking periods of the LHC. The integrated luminosities are 4.9, 19.7, and $2.3\,\mathrm{fb}^{-1}$ at centre of mass energies of 7, 8, and 13 TeV, respectively. The uncertainties in the integrated luminosity measurements are 2.2%, 2.6%, and 2.7% at 7 [38], 8 [39], and 13 TeV [40], respectively.

Simulated ggH and qqH events are generated with POWHEG 1.0 (POWHEG 2.0) [41–43] interfaced with PYTHIA 6.4 [44] (PYTHIA 8.1 [45]) at 7 and 8 (13) TeV. The inclusive cross section for ggH production is calculated to next-to-next-to-next-to-leading order ($\mathrm{N^3LO}$) precision in quantum chromodymanics (QCD) and next-to-leading order (NLO) in EW theory [46]. The qqH inclusive cross section calculation uses next-to-next-to-leading order (NNLO) QCD and NLO EW precision [47]. In the 8 TeV sample, the p_T distribution of the Higgs boson in the ggH process is reweighted to match the NNLO plus next-to-next-to-leading-logarithmic (NNLL) prediction from HRES2.1 [48, 49]. The event generation at 13 TeV is tuned so that the p_T distribution agrees between POWHEG 2.0 and HRES2.1. Associated VH production is generated using PYTHIA 6.4 (PYTHIA 8.1) at 7 and 8 (13) TeV and normalised to an inclusive cross section calculated at NNLO QCD and NLO EW precision [47]. The expected contribution from $\mathrm{gg} \to \mathrm{ZH}$ production is estimated using events generated with POWHEG 2.0 interfaced with PYTHIA 8.1. All signal processes are generated assuming a Higgs boson mass of 125 GeV, consistent with the combined ATLAS and CMS measurement of the Higgs boson mass [50]. The SM Higgs boson cross sections at 125 GeV and their uncertainties for all production mechanisms are taken from ref. [51] at all centre-of-mass energies. A summary of the simulation used for the different signal processes is given in table 1.

The majority of background samples, including W+jets, Z+jets, $t\bar{t}$, and triboson production, are generated using MADGRAPH 5.1 [52] (MADGRAPH 5_aMC@NLO2.2 [53]) with leading order (LO) precision, interfaced with PYTHIA 6.4 (PYTHIA 8.1) for hadronisation and fragmentation in the 7 and 8 (13) TeV analyses. Single top quark event samples are produced using POWHEG 1.0 [54] and diboson samples are generated using PYTHIA 6.4 (PYTHIA 8.1) at 7 and 8 (13) TeV. QCD multijet events are generated using either PYTHIA

Production process	incl. cross section precision	7 TeV	8 TeV	13 TeV
ggH	N³LO (QCD), NLO (EW)	POWHEG 1.0+PYTHIA 6.4	POWHEG 1.0+PYTHIA 6.4	POWHEG 2.0+PYTHIA 8.1
qqH	NNLO (QCD), NLO (EW)	POWHEG 1.0+PYTHIA 6.4	POWHEG 1.0+PYTHIA 6.4	POWHEG 2.0+PYTHIA 8.1
VH qq → VH	NNLO (QCD), NLO (EW)	PYTHIA 6.4	PYTHIA 6.4	PYTHIA 8.1
gg → ZH	NNLO (QCD), NLO (EW)	POWHEG 2.0+PYTHIA 8.1	POWHEG 2.0+PYTHIA 8.1	POWHEG 2.0+PYTHIA 8.1

Table 1. Simulations used for the different Higgs boson production processes in the 7, 8 and 13 TeV analyses. The p_{T} distribution of the ggH production is modified in the 8 TeV simulation to match that predicted with HRES as described in the text. The accuracy of the inclusive cross section used for each process is shown, details of which can be found in the text.

6.4 or MADGRAPH 5_aMC@NLO2.2, depending on the analysis. All signal and background samples use the CTEQ6L [55] (NNPDF3.0 [56]) parton distribution functions (PDFs) at 7 and 8 (13) TeV. The underlying event simulation is done using parameters from the Z2* tune [57, 58] and the CUETP8M1 tune [58] for PYTHIA 6.4 and PYTHIA 8.1, respectively.

The interactions of all final-state particles with the CMS detector are simulated with GEANT4 [59]. The simulated samples include PU interactions with the multiplicity of reconstructed primary vertices matching that in the relevant data sets. An uncertainty of 5% in the total inelastic pp cross section is propagated to the PU distribution and is treated as correlated between the data-taking periods.

4 Analyses included in the combination

The characteristic signature of invisible Higgs boson decays for all of the included searches is a large $E_{\mathrm{T}}^{\mathrm{miss}}$, with the jets or leptons recoiling against the $\vec{p}_{\mathrm{T}}^{\mathrm{miss}}$, consistent with one of the production topologies. In order to reduce the contributions expected from the SM backgrounds, the properties of the visible recoiling system are exploited. The events are divided into several exclusive categories designed to target a particular production mode. A summary of the analyses included in the combination and the expected signal composition in each of them are given in table 2. The VBF search at 8 TeV used in this paper improves on the previous analysis [17] by using additional data samples from high-rate triggers installed in CMS in 2012. These triggers wrote data to a special stream, and the events were reconstructed during the long shutdown of the LHC in 2013 [60]. The limit setting procedure has also been updated to allow for a common approach between the 8 and 13 TeV analyses. The Z($\ell^+\ell^-$) search at 7 and 8 TeV is identical to the one described in ref. [17] but is described in this paper to allow for comparison to the 13 TeV analysis. Both the V(jj) and monojet analyses at 8 TeV are re-interpretations of a generic search for DM production described in ref. [61] with minor modifications to the selection of events and limit extraction procedure. In addition to the channels described in the following sections, an 8 TeV analysis targeting ZH production in which the Z boson decays to a $b\bar{b}$ pair, described in ref. [17], is included in this combination.

The signal in the VBF analysis is expected to be dominated by qqH production and the expected signals in the Z($\ell^+\ell^-$) and Z($b\bar{b}$) analyses are composed entirely of ZH production. In contrast, the V(jj) and monojet analyses, which target events with a central, Lorentz-

Analysis	Final state	Int. $\mathcal{L}$ (fb^{-1})			Expected signal composition (%)	
		7 TeV	8 TeV	13 TeV	7 or 8 TeV	13 TeV
qqH-tagged	VBF jets	—	19.2 [17]	2.3	7.8 (ggH), 92.2 (qqH)	9.1 (ggH), 90.9 (qqH)
VH-tagged	Z($\ell^+\ell^-$)	4.9 [17]	19.7 [17]	2.3	100 (ZH)	
	Z(b$\bar{\text{b}}$)	—	18.9 [17]	—	100 (ZH)	
	V(jj)	—	19.7 [61]	2.3	25.1 (ggH), 5.1 (qqH), 23.0 (ZH), 46.8 (WH)	38.7 (ggH), 7.1 (qqH), 21.3 (ZH), 32.9 (WH)
ggH-tagged	Monojet	—	19.7 [61]	2.3	70.4 (ggH), 20.4 (qqH), 3.5 (ZH), 5.7 (WH)	69.3 (ggH), 21.9 (qqH), 4.2 (ZH), 4.6 (WH)

Table 2. Summary of the expected composition of production modes of a Higgs boson with a mass of 125 GeV in each analysis included in the combination. The relative contributions assume SM production cross sections.

boosted jet, contain a mixture of the different production modes. This is due to the limited discrimination power of the jet identification used to categorise these events. As shown in table 2, the signal composition is similar across the 7 or 8, and 13 TeV data sets. In the V(jj) analysis the ZH contribution is larger, relative to the WH contribution, in the 13 TeV analysis compared to the 8 TeV analysis. This is because the lepton veto requirement is less efficient at removing leptonic Z boson decays in the case where the lepton pair is produced at high Lorentz boost causing the isolation cones of the two leptons to overlap more often at a centre-of-mass energy of 13 TeV compared to 8 TeV. Each analysis has been optimised separately for the specific conditions and integrated luminosity of the 7, 8, and 13 TeV data sets leading to differences in the kinematic requirements across the data sets. These differences are discussed in the following sections.

4.1 The VBF analysis

The qqH Higgs boson production mode is characterised by the presence of two jets with a large separation in η and a large invariant mass (m_{jj}). The selection of events targeting qqH production exploits this distinctive topology to give good discrimination between the invisible decays of a Higgs boson and the large SM backgrounds. The contributions from the dominant Z($\nu\nu$)+jets and W($\ell\nu$)+jets backgrounds and the QCD multijet backgrounds are estimated using control regions in data. A simultaneous fit to the yields in the signal and control regions is performed to extract any potential signal and place upper limits on $\mathcal{B}(\text{H} \to \text{inv})$.

4.1.1 Event selection

Events are selected online using a dedicated VBF trigger, in both the 8 and 13 TeV data sets, with thresholds optimised for the instantaneous luminosities during each data-taking period. The trigger requires a forward-backward pair of jets with a pseudorapidity separation of $|\Delta\eta(\text{j}_1, \text{j}_2)| > 3.5$ and a large invariant mass. For the majority of the 8 TeV data-taking period the thresholds used were $p_\text{T}^{\text{j}_1}$, $p_\text{T}^{\text{j}_2} > 30$ or $35\,\text{GeV}$, depending on the

	8 TeV	13 TeV
$p_T^{j_1}$	>50 GeV	>80 GeV
$p_T^{j_2}$	>45 GeV	>70 GeV
m_{jj}	>1200 GeV	>1100 GeV
E_T^{miss}	>90 GeV	>200 GeV
$S(E_T^{miss})$	>4$\sqrt{\text{GeV}}$	—
$\min \Delta\phi(\vec{p}_T^{\,miss}, j)$	>2.3	
$\Delta\eta(j_1, j_2)$	>3.6	

Table 3. Event selections for the VBF invisible Higgs boson decay search at 8 and 13 TeV.

LHC conditions, and $m_{jj} > 700$ GeV. For the 13 TeV data set, these were modified to $p_T > 40$ GeV and $m_{jj} > 600$ GeV. In addition, the trigger requires the presence of missing transverse energy, reconstructed using the ECAL and HCAL information only. The thresholds were $E_T^{miss} > 40\,(140)$ GeV at 8 (13) TeV. The efficiency of the trigger was measured as a function of the main selection variables: $p_T^{j_1}$, $p_T^{j_2}$, m_{jj}, and E_T^{miss}. A parameterisation of this efficiency is then applied as a weight to simulated events. The subsequent selection after the full reconstruction is designed to maintain a trigger efficiency of greater than 80%.

The selection of events is optimised for VBF production of the Higgs boson with a mass of 125 GeV, decaying to invisible particles. Events are required to contain at least two jets within $|\eta| < 4.7$ with pseudorapidities of opposite sign, separated by $|\Delta\eta(j_1, j_2)| > 3.6$. The two jets in the event with the highest p_T satisfying this requirement form the dijet pair. The leading and subleading jets in this pair are required to have $p_T^{j_1} > 50\,(80)$ GeV, $p_T^{j_2} > 45\,(70)$ GeV, and dijet invariant mass $m_{jj} > 1200\,(1100)$ GeV at 8 (13) TeV. Events are required to have $E_T^{miss} > 90\,(200)$ GeV at 8 (13) TeV.

For the 8 TeV dataset, an additional requirement is set on an approximate missing transverse energy significance variable $S(E_T^{miss})$ defined as the ratio of E_T^{miss} to the square root of the scalar sum of the transverse energy of all PF objects in the event [62]. Selected events are required to satisfy $S(E_T^{miss}) > 4\sqrt{\text{GeV}}$.

In order to reduce the large backgrounds from QCD multijet production, the jets in the event are required to be recoiling against the $\vec{p}_T^{\,miss}$. The azimuthal angle between $\vec{p}_T^{\,miss}$ and each jet in the event, $\Delta\phi(\vec{p}_T^{\,miss}, j)$, is determined. The minimum value of this angle $\min\Delta\phi(\vec{p}_T^{\,miss}, j)$ is required to be greater than 2.3. Finally, events containing at least one muon or electron with $p_T > 10$ GeV are rejected to suppress backgrounds from leptonic decays of the vector boson.

A summary of the event selection used in the 8 and 13 TeV data sets is given in table 3. Figure 3 shows the distribution of $\Delta\eta(j_1, j_2)$ and m_{jj} in data and the predicted background contributions after the selection. The contribution expected from a Higgs boson with a mass of 125 GeV, produced assuming SM cross sections and decaying to invisible particles with 100% branching fraction, is also shown. The backgrounds have been normalised using the results of a simultaneous fit, as described in section 4.1.2.
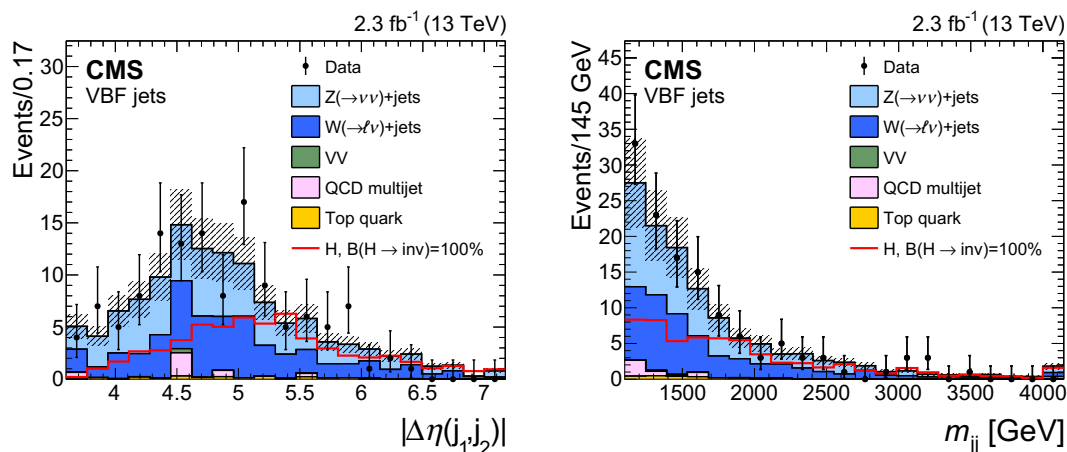
Figure 3. Distributions of (left) $\Delta\eta(j_1, j_2)$ and (right) m_{jj} in events selected in the VBF analysis for data and simulation at 13 TeV. The background yields are scaled to their post-fit values, with the total post-fit uncertainty represented as the black hatched area. The last bin contains the overflow events. The expected contribution from a Higgs boson with a mass of 125 GeV, produced with the SM cross section and decaying to invisible particles with 100% branching fraction, is overlaid.

4.1.2 Background estimation

The dominant backgrounds to this search arise from $Z(\nu\nu)$+jets events and $W(\ell\nu)$+jets events with the charged lepton outside of the detector acceptance or not identified. These backgrounds are estimated using data control regions, in which a Z or W boson, produced in association with the same dijet topology, decays to well-identified charged leptons. These control regions are designed to be as similar to the signal region as possible to limit the extrapolation required between different kinematic phase spaces. An additional control region, enriched in QCD multijet events, is defined to estimate the contribution arising due to mismeasured jet energies causing apparent E_T^{miss}. Additional smaller contributions due to diboson, $t\bar{t}$, and single top quark production are estimated directly from simulation.

A dimuon control region is defined, enriched in $Z \to \mu^+\mu^-$ events, requiring a pair of oppositely charged muons with $p_T > 20$ GeV, $|\eta| < 2.1$, and an invariant mass $m_{\mu\mu}$ in the range 60–120 GeV. Three single-lepton regions (one enriched in each of the $W \to e\nu$, $W \to \mu\nu$, and $W \to \tau\nu$ processes) are defined by removing the lepton veto and requiring exactly one isolated lepton, with $p_T > 20$ GeV, of a given flavour, and no leptons of any other flavour. The lepton is required to be within $|\eta| < 2.1$, 2.4, or 2.3 for the single-muon, single-electron, or single τ lepton region, respectively. The remaining jets and E_T^{miss} criteria are identical to the signal region, except in the $W \to \tau\nu$ control region where the $\min \Delta\phi(\vec{p}_T^{\,miss}, j)$ criterion is relaxed to $\min \Delta\phi(\vec{p}_T^{\,miss}, j) > 1$, taking the minimum over the leading two jets only, to ensure QCD multijet events are suppressed, while retaining a sufficient number of events in the control region. Additionally, a requirement that $\min \Delta\phi(\vec{p}_T^{\,miss}, j) < 2.3$ is applied to maintain an orthogonal selection to the signal region.

Finally, additional control regions are defined in data that are identical to the signal region selection except for the requirement on $\min \Delta\phi(\vec{p}_{\mathrm{T}}^{\mathrm{miss}}, \mathrm{j})$. In the 8 TeV analysis, a two-step procedure is used in which two control regions are defined. The first control region is defined by $\min \Delta\phi(\vec{p}_{\mathrm{T}}^{\mathrm{miss}}, \mathrm{j}) < 1$ and is used to determine the distribution of $S(E_{\mathrm{T}}^{\mathrm{miss}})$ for QCD multijet events once the contributions from other backgrounds are subtracted. The distribution is normalised using events in a second region defined as $3 < S(E_{\mathrm{T}}^{\mathrm{miss}}) < 4\sqrt{\mathrm{GeV}}$ and $1 < \min \Delta\phi(\vec{p}_{\mathrm{T}}^{\mathrm{miss}}, \mathrm{j}) < 2$, where the signal contribution is expected to be negligible. The integral of the normalised distribution in the region $S(E_{\mathrm{T}}^{\mathrm{miss}}) > 4\sqrt{\mathrm{GeV}}$ provides the estimate of the QCD multijet event contribution in the signal region. In the 13 TeV analysis, an independent control region is defined by a requirement of $\min \Delta\phi(\vec{p}_{\mathrm{T}}^{\mathrm{miss}}, \mathrm{j}) < 0.5$ to enrich the QCD multijet contribution. Systematic uncertainties of 80% and 100% are included at 8 and 13 TeV to account for potential biases in the extrapolation to the signal region.

Several sources of experimental systematic uncertainties are included in the predictions of the background components. The dominant ones are the jet energy scale and resolution [31] uncertainties, which are also propagated to the calculation of the $E_{\mathrm{T}}^{\mathrm{miss}}$, resulting in uncertainties of up to 8% in the expected background yields. Smaller uncertainties are included to account for the PU description and lepton reconstruction efficiencies. Due to the looser selection applied in the $\mathrm{W} \to \tau\nu$ control region compared to the signal region, an additional systematic uncertainty of 20% in the prediction of the $\mathrm{W} \to \tau\nu$ contribution is included. Finally, additional cross section uncertainties of 7% (10%) [63–67] for diboson production and 10% (20%) [68–70] for the top quark background at 8 (13) TeV are included.

In order to estimate the background contributions, a maximum likelihood fit is performed simultaneously across each of the control regions, taking the expected background yields from simulation and observed event counts as inputs to the fit. Two scale factors are included as free parameters in the fit, one scaling both the W+jets and Z+jets processes and one scaling the QCD multijet yields across all of the regions. The fit is thereby able to constrain the contributions from W+jets, Z+jets, and QCD multijets directly from data.

The ratio of $\mathrm{W}(\ell\nu)$+jets to $\mathrm{Z}(\nu\nu)$+jets is calculated using simulated samples, generated at LO. Separate samples are produced for the production of the jets through quark-gluon vertices (QCD) and production through quark-vector-boson vertices (EW). A theoretical systematic uncertainty in the expected ratio of the $\mathrm{W}(\ell\nu)$+jets to $\mathrm{Z}(\nu\nu)$+jets yields is derived by comparing LO and NLO predictions after applying the full VBF kinematic selection using events generated with MadGraph 5_aMC@NLO 2.2 interfaced with pythia 8.1, excluding events produced via VBF. A difference of 30% is observed between the ratios predicted by the LO and NLO calculations and is included as a systematic uncertainty in the ratio of the W+jets to Z+jets contributions. The ratio of the production cross sections of $\mathrm{W}(\ell\nu)$+jets to $\mathrm{Z}(\nu\nu)$+jets through EW vertices is compared at NLO and LO precision using vbf@nlo2.7 [71, 72] and found to agree within the 30% systematic uncertainty assigned.

The observed yields in data for each of the control regions in the 13 TeV data set, and the expected contributions from the backgrounds after the fit ignoring the signal region events, are given in table 4.

Process		Signal Region	Control regions				
			Single e	Single μ	Single τ	$\mu^+\mu^-$	QCD
Z($\mu^+\mu^-$)+jets	QCD	—	—	—	—	4.2 ± 1.1	—
	EW	—	—	—	—	2.0 ± 0.7	—
Z($\nu\nu$)+jets	QCD	47 ± 12	—	—	—	—	—
	EW	21 ± 7	—	—	—	—	—
W($\mu\nu$)+jets	QCD	13 ± 2	—	53 ± 5	0.4 ± 0.2	—	45 ± 5
	EW	4.3 ± 0.8	—	27 ± 3	—	—	6.0 ± 0.9
W(eν)+jets	QCD	9.3 ± 1.5	17 ± 3	—	0.2 ± 2.2	—	39 ± 4
	EW	5.4 ± 1.1	7.8 ± 1.3	—	0.2 ± 0.1	—	6.1 ± 1.0
W($\tau\nu$)+jets	QCD	13 ± 2	0.06 ± 0.06	—	12 ± 2	—	74 ± 9
	EW	5.5 ± 1.2	—	—	5.1 ± 1.2	—	24 ± 3
Top quark		2.3 ± 0.4	1.5 ± 0.3	6.8 ± 0.9	7.1 ± 1.0	0.22 ± 0.06	82 ± 11
QCD multijet		3 ± 23	—	5 ± 3	0.4 ± 0.3	—	1200 ± 170
Dibosons		0.7 ± 0.3	0.4 ± 0.4	0.8 ± 0.4	—	0.02 ± 0.02	1.8 ± 0.7
Total bkg.		125 ± 28	27 ± 3	91 ± 8	25 ± 4	6.4 ± 1.4	1500 ± 170
Data		126	29	89	24	7	1461
Signal	qqH	53.6 ± 4.9					
$m_H = 125\,\mathrm{GeV}$	ggH	5.4 ± 3.6					

Table 4. Post-fit yields for the control regions and signal region of the VBF analysis using the 13 TeV data set. The fit ignores the constraints due to the data in the signal region. For the W and Z processes, jet production through QCD or EW vertices are listed as separate entries. The signal yields shown assume SM ggH and qqH production rates for a Higgs boson with a mass of 125 GeV, decaying to invisible particles with $\mathcal{B}(\mathrm{H} \to \mathrm{inv}) = 100\%$.

4.2 The Z($\ell^+\ell^-$) analysis

The ZH production mode, where the Z boson decays to a pair of charged leptons, has a smaller cross section than qqH but a clean final state with lower background. The search targets events with a pair of same-flavour, opposite-charge leptons ($l = \mathrm{e}, \mu$), consistent with a leptonic Z boson decay, produced in association with a large $E_\mathrm{T}^\mathrm{miss}$. The background is dominated by the diboson processes, $\mathrm{ZZ} \to \ell\ell\nu\nu$ and $\mathrm{WZ} \to \ell\nu\ell\ell$, which contribute roughly 70% and 25% of the total background, respectively.

In the 7 and 13 TeV data sets the sensitivity of the search is enhanced by using the distribution of the transverse mass of the dilepton-$E_\mathrm{T}^\mathrm{miss}$ system m_T, defined as

$$m_\mathrm{T} = \sqrt{2p_\mathrm{T}^{\ell\ell} E_\mathrm{T}^\mathrm{miss} \left[1 - \cos \Delta\phi(\ell\ell, \vec{p}_\mathrm{T}^\mathrm{miss})\right]},$$

where $p_\mathrm{T}^{\ell\ell}$ is the transverse momentum of the dilepton system and $\Delta\phi(\ell\ell, \vec{p}_\mathrm{T}^\mathrm{miss})$ is the azimuthal angle between the dilepton system and the missing transverse momentum vector. In the 8 TeV data set, a two-dimensional fit is performed to the distributions of m_T and the azimuthal angle between the two leptons $\Delta\phi(\ell, \ell)$ to exploit the increased statistical precision available in that data set [17].

	7 and 8 TeV	13 TeV
$p_T^{e,\mu}$	\>20 GeV	
$m_{\ell\ell}$	76–106 GeV	
$\Delta\phi(\ell,\ell)$	—	$<\pi/2$
E_T^{miss}	\>120 GeV	\>100 GeV
$\Delta\phi(\ell\ell,\vec{p}_T^{\,miss})$	\>2.7	\>2.8
$\Delta\phi(\vec{p}_T^{\,miss},j)$	—	\>0.5
$|E_T^{miss} - p_T^{\ell\ell}|/p_T^{\ell\ell}$	<0.25	<0.4
m_T	\>200 GeV	

Table 5. Event selections for the $Z(\ell^+\ell^-)$ invisible Higgs boson search using the 7, 8, and 13 TeV data sets. The $\Delta\phi(\vec{p}_T^{\,miss},j)$ requirement is applied only in the 1-jet category.

4.2.1 Event selection

Events for this channel are recorded using double-electron and double-muon triggers, with thresholds of $p_T^e > 17\,(12)\,$GeV and $p_T^\mu > 17\,(8)\,$GeV at 13 TeV and $p_T^{e,\mu} > 17\,(8)\,$GeV at 7 and 8 TeV, for the leading (subleading) electron or muon, respectively. Single-electron and single-muon triggers are also included in order to recover residual trigger inefficiencies.

Selected events are required to have two well-identified, isolated leptons with the same flavour and opposite charge (e^+e^- or $\mu^+\mu^-$), each with $p_T > 20\,$GeV, and an invariant mass within the range 76–106 GeV. In the 13 TeV analysis, the $Z/\gamma^* \to \ell^+\ell^-$ background is substantially suppressed by requiring $\Delta\phi(\ell,\ell) < \pi/2$. As little hadronic activity is expected in the $Z(\ell\ell)$H channel, events with more than one jet with $p_T > 30\,$GeV are rejected. Events containing a muon with $p_T > 3\,$GeV and a b jet with $p_T > 30\,$GeV are vetoed to reduce backgrounds from top quark production. Diboson backgrounds are suppressed by rejecting events containing additional electrons or muons with $p_T > 10\,$GeV. In the 13 TeV analysis, events containing a τ lepton with $p_T > 20\,$GeV are vetoed to suppress the contributions from WZ production.

The remainder of the selection has been optimised for a Higgs boson with a mass of 125 GeV, produced in the $Z(\ell\ell)$H production mode. As a result of this optimisation, events are required to have $E_T^{miss} > 120\,(100)\,$GeV, $\Delta\phi(\ell\ell,\vec{p}_T^{\,miss}) > 2.7\,(2.8)$, and $|E_T^{miss}-p_T^{\ell\ell}|/p_T^{\ell\ell} < 0.25\,(0.4)$, in the 7 and 8 (13) TeV data sets. Finally, the events are required to have $m_T > 200\,$GeV. A summary of the event selection used for the 7, 8, and 13 TeV data sets is given in table 5.

The selected events are separated into two categories, events that contain no jets with $p_T > 30\,$GeV and $|\eta| < 4.7$, and events that contain exactly one such jet. An additional selection requiring $\Delta\phi(\vec{p}_T^{\,miss},j) > 0.5$ is applied in the 1-jet category at 13 TeV which significantly reduces the contribution from Z+jets events.

The distributions of m_T for selected events in data and simulation, combining electron and muon events, for the 0-jet and 1-jet categories at 13 TeV are shown in figure 4.
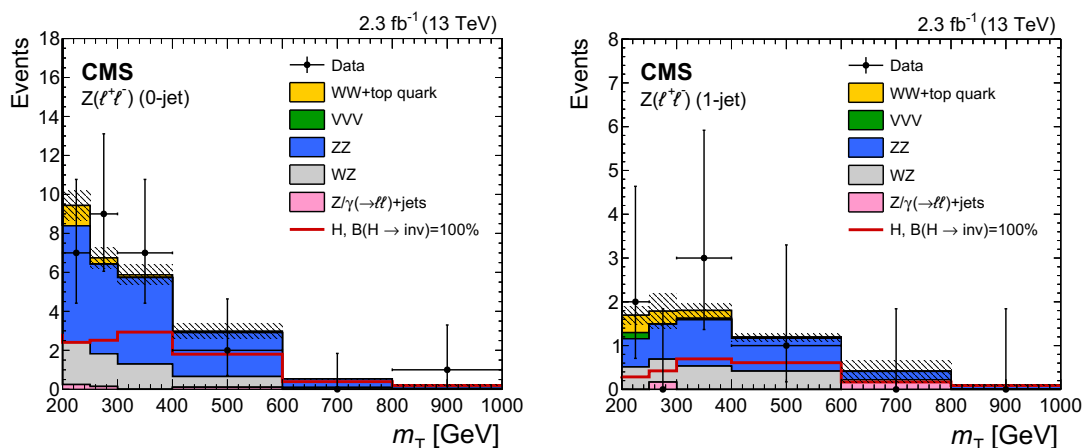
Figure 4. Distributions of m_T in data and simulation for events in the (left) 0-jet and (right) 1-jet categories of the $Z(\ell^+\ell^-)$ analysis at 13 TeV, combining dielectron and dimuon events. The background yields are normalised to 2.3 fb^{-1}. The shaded bands represent the total statistical and systematic uncertainties in the backgrounds. The horizontal bars on the data points represent the width of the bin centred at that point. The expectation from a Higgs boson with a mass of 125 GeV, from ZH production, decaying to invisible particles with a 100% branching fraction is shown in red.

4.2.2 Background estimation

The dominant backgrounds, $ZZ \to \ell\ell\nu\nu$ and $WZ \to \ell\nu\ell\ell$, are generated at NLO using POWHEG 2.0, for production via $q\bar{q}$. Corrections are applied to account for higher-order QCD and EW effects which are roughly 10–15% each but with opposite sign. The contribution from $gg \to ZZ$ is estimated using MCFM7.0 [73]. Uncertainties due to missing higher-order corrections for these processes are evaluated by varying the renormalisation and factorisation scales up and down by a factor of two, yielding systematic uncertainties between 4 and 10%. A 2% uncertainty is added to account for the jet category migration due to uncertainties in the PDFs used in the signal generation, calculated following the procedures outlined in ref. [74]. Additional uncertainties are included in the $q\bar{q} \to ZZ$ event yield to account for the uncertainties in the higher-order corrections applied.

The Z+jets background is estimated using a data control region dominated by single-photon production in association with jets (γ+jets). The γ+jets events have similar jet kinematics to $Z/\gamma^*(\ell^+\ell^-)$+jets, but with a much larger production rate. The γ+jets events are weighted, as a function of the photon p_T, to match the distribution observed in $Z/\gamma^*(\ell^+\ell^-)$+jets events in data. This accounts for the dependence of the E_T^{miss} on the hadronic activity. A systematic uncertainty of 100% is included in the final Z+jets background estimate to account for the limited number of events at large p_T in the data used to weight the γ+jets events.

The remaining, nonresonant backgrounds are estimated using a control sample selecting pairs of leptons of different flavour and opposite charge ($e^\pm\mu^\mp$) that pass all of the signal region selections. These backgrounds consist mainly of leptonic W boson decays in $t\bar{t}$ and tW processes, and WW events. Additionally, leptonic τ lepton decays contribute

to these backgrounds. As the branching fraction to the $e^{\pm}\mu^{\mp}$ final states is twice that of the e^+e^- or $\mu^+\mu^-$ final states, the $e^{\pm}\mu^{\mp}$ control region provides precise estimates of the nonresonant backgrounds. In the 13 TeV analysis, the contribution from the nonresonant backgrounds is given by

$$N_{\ell\ell}^{\text{bkg}} = N_{e\mu}^{\text{data}}(k_{ee/\mu\mu} + 1/k_{ee/\mu\mu})/2,$$

where $N_{e\mu}^{\text{data}}$ is the number of events in the $e^{\pm}\mu^{\mp}$ control region after subtracting other backgrounds and $k_{ee/\mu\mu} = \sqrt{N_{ee}/N_{\mu\mu}}$ is a correction factor accounting for the differences in acceptance and efficiency for electrons and muons, measured using $Z/\gamma^* \to e^+e^-$ and $Z/\gamma^* \to \mu^+\mu^-$ events in data. An uncertainty of 70% in the estimated yield of the nonresonant backgrounds is included to account for the statistical and systematic uncertainties of the extrapolation from the $e^{\pm}\mu^{\mp}$ control region. A similar method using sideband regions around the Z boson mass peak was used to estimate these backgrounds in the 8 TeV analysis, as described in ref. [17]. This method was also used in the 13 TeV analysis as a cross check and the differences between the results of the two methods of 10–15% are included as additional systematic uncertainties.

Additional uncertainties in the background estimates arise from uncertainties in the lepton efficiencies, momentum scale, jet energy scale and resolution, and E_T^{miss} energy scale and resolution. Each of these contributes around 2% uncertainty in the normalisation of the dominant backgrounds. Statistical uncertainties are included for all simulated samples. These uncertainties are propagated as both shape and normalisation variations of the predicted m_T distributions.

The numbers of expected and observed events for the 0-jet and 1-jet categories in the 13 TeV analysis are given in table 6. The signal yield assumes the SM ZH production rate for a Higgs boson with a mass of 125 GeV decaying to invisible particles with 100% branching fraction.

4.3 The V(jj) and monojet analyses

Searches for final states with central jets and E_T^{miss} suffer from large backgrounds. However, the ggH mode and the VH associated mode, in which the vector boson decays hadronically, have relatively large signal contributions despite the tight requirements on the jets. The search strategies for the VH mode, in which the vector boson decays hadronically, and ggH modes are very similar, targeting events with large E_T^{miss}, with the $\vec{p}_T^{\text{miss}}$ recoiling against jets from either gluon radiation or a hadronically decaying vector boson. Events are divided into two categories, depending on the jet properties. The dominant backgrounds arise from $Z(\nu\nu)$+jets and $W(\ell\nu)$+jets events, accounting for 90% of the total background. These backgrounds are estimated using control regions in data and a simultaneous fit to the E_T^{miss} distribution of the events across all regions is performed to extract a potential signal.

4.3.1 Event selection

The data set is collected using a suite of triggers with requirements on E_T^{miss} and hadronic activity. In the 8 TeV analysis two triggers are used: the first requires $E_T^{\text{miss}} > 120$ GeV,

Process	0 jets		1 jet	
	$\mu^+\mu^-$	e^+e^-	$\mu^+\mu^-$	e^+e^-
ZH, $m_H = 125\,\text{GeV}$	5.97 ± 0.55	4.27 ± 0.39	1.29 ± 0.20	0.98 ± 0.15
$Z/\gamma^*(\ell^+\ell^-)$+jets	0.45 ± 0.45	0.30 ± 0.30	0.45 ± 0.45	0.30 ± 0.30
$ZZ \to \ell\ell\nu\nu$	10.4 ± 1.14	7.46 ± 0.81	2.04 ± 0.31	1.49 ± 0.23
$WZ \to \ell\nu\ell\ell$	3.42 ± 0.28	2.40 ± 0.19	1.04 ± 0.10	1.00 ± 0.10
Top/WW/$\tau\tau$	0.69 ± 0.23	0.88 ± 0.29	0.44 ± 0.22	0.26 ± 0.13
VVV	—	—	0.13 ± 0.06	0.07 ± 0.03
Total background	15.0 ± 1.28	11.0 ± 0.93	4.10 ± 0.60	3.12 ± 0.41
Data	18	8	5	1

Table 6. Predicted signal and background yields and observed number of events after full selection in the 13 TeV $Z(\ell^+\ell^-)$-tagged analysis. The numbers are given for the 0-jet and 1-jet categories, separately for the e^+e^- and $\mu^+\mu^-$ final states. The uncertainties include statistical and systematic components. The signal prediction assumes a SM ZH production rate for a Higgs boson with the mass of 125 GeV and a 100% branching fraction to invisible particles.

while the second requires $E_T^{\text{miss}} > 95$ or $105\,\text{GeV}$, depending on the data-taking period, together with a jet of $p_T > 80\,\text{GeV}$ and $|\eta| < 2.6$. In the 13 TeV data set, the trigger requires $E_T^{\text{miss}} > 90\,\text{GeV}$ and $H_T^{\text{miss}} > 90\,\text{GeV}$, where H_T^{miss} is defined as the magnitude of the vector sum of the p_T of all jets with $p_T > 20\,\text{GeV}$. In both 8 and 13 TeV data sets the calculation of E_T^{miss} does not include muons, allowing for the same triggers to be used in the signal, single-muon and dimuon control regions. For events selected for the analysis, the trigger efficiency is found to be greater than 99% (98%) at 8 (13) TeV.

To reduce the QCD multijet background the events in the 8 TeV analysis that do not satisfy the requirement that the angle between the $\vec{p}_T^{\text{miss}}$ and the leading jet $\Delta\phi(\vec{p}_T^{\text{miss}}, \text{j}) > 2$ are removed. In the 13 TeV data set the requirement is instead $\min \Delta\phi(\vec{p}_T^{\text{miss}}, \text{j}) > 0.5$, where the minimum is over the four leading jets in the event. Events in the signal regions of the 8 (13) TeV analysis are vetoed if they contain an electron or muon with $p_T > 10\,\text{GeV}$, a photon with $p_T > 10\,(15)\,\text{GeV}$, or a τ lepton with $p_T > 18\,(15)\,\text{GeV}$. Backgrounds from top quark decays are suppressed by applying a veto on events containing a b jet with $p_T > 15\,\text{GeV}$.

Selected events are classified by the topology of the jets in order to distinguish initial- or final-state radiation from hadronic vector boson decays. This results in two exclusive event categories to target two channels: the monojet and V(jj). If the vector boson decays hadronically and has sufficiently high p_T, its hadronic decay products are captured by a single reconstructed large-radius jet. Events in the V(jj) channel are required to have $E_T^{\text{miss}} > 250\,\text{GeV}$ and contain a reconstructed $R = 0.8$ jet with $p_T > 200\,(250)\,\text{GeV}$ and $|\eta| < 2.0\,(2.4)$ in the 8 (13) TeV analysis. Additional requirements are included to better identify jets from the decay of a vector boson by using the "subjettiness" quantity τ_2/τ_1, as defined in refs. [75, 76], which identifies jets with a two subjet topology, and the pruned jet mass (m_{prune}) [77]. The τ_2/τ_1 ratio is required to be smaller than 0.5 (0.6) and m_{prune} is required to be in the range 60–110 (65–105) GeV in the 8 (13) TeV analysis. The optimi-

	8 TeV		13 TeV	
	V(jj)	Monojet	V(jj)	Monojet
p_T^j	>200 GeV	>150 GeV	>250 GeV	>100 GeV
$\|\eta\|^\mathrm{j}$	<2		<2.4	<2.5
$E_\mathrm{T}^\mathrm{miss}$	>250 GeV	>200 GeV	>250 GeV	>200 GeV
τ_2/τ_1	<0.5	—	<0.6	—
m_prune	60–110 GeV	—	65–105 GeV	—
$\min\Delta\phi(\vec{p}_\mathrm{T}^\mathrm{miss}, \mathrm{j})$	>2 rad		>0.5 rad	
N_j	=1		—	

Table 7. Event selections for the V(jj) and monojet invisible Higgs boson decay searches using the 8 and 13 TeV data sets. The requirements on p_T^j and $|\eta|^\mathrm{j}$ refer to the highest p_T (large-radius) jet in the monojet (V(jj)) events. The 8 TeV analysis uses only the leading jet in the definition of $\min\Delta\phi(\vec{p}_\mathrm{T}^\mathrm{miss}, \mathrm{j})$. In the 8 TeV number of jets N_j selection, events with one additional jet are allowed if this additional jet falls within $\Delta\phi$ of the leading jet as described in the text.

sation of the selection for VH production is performed independently for the 8 and 13 TeV data sets.

If an event fails the V(jj) selection, it can instead be included in the monojet channel. Events in this channel are required to contain at least one anti-k_T jet, reconstructed with cone size 0.5 (0.4), with $p_\mathrm{T} > 150$ (100) GeV and $|\eta| < 2.0$ (2.5) in the 8 (13) TeV analysis. In the 8 TeV analysis, only events with up to two jets are included in the V(jj) and monojet categories, provided that the separation of the second jet from the leading jet in azimuthal angle satisfies $\Delta\phi < 2$. For the purposes of this requirement, only jets reconstructed with the anti-k_T algorithm using a cone size of 0.5 are counted beyond the leading jet in the V(jj) channel. This requirement on the maximum number of jets N_j was dropped for the 13 TeV analysis to increase the signal acceptance. Finally, events are required to have $E_\mathrm{T}^\mathrm{miss} > 200$ GeV.

A summary of the event selection for the V(jj) and monojet categories is given in table 7. In addition to this selection, events that pass the corresponding VBF selection are vetoed to avoid an overlap with the VBF search.

4.3.2 Background estimation

The dominant Z($\nu\nu$)+jets and W($\ell\nu$)+jets backgrounds are estimated from control regions in data consisting of dimuon, single-muon, and γ+jets events. In the 13 TeV analysis, additional control regions consisting of dielectron and single-electron events are used. The $E_\mathrm{T}^\mathrm{miss}$ in each control region is redefined to mimic the $E_\mathrm{T}^\mathrm{miss}$ distribution of the Z($\nu\nu$)+jets and W($\ell\nu$)+jets backgrounds in the signal region by excluding the leptons or the photon from the computation of $E_\mathrm{T}^\mathrm{miss}$.

A dimuon control region is defined by selecting events that contain two opposite-sign muons with $p_\mathrm{T}^{\mu_1, \mu_2} > 10$ (20), 10 GeV at 8 (13) TeV and an invariant mass between 60 and 120 GeV. A single-muon control region is defined by selecting events with an isolated muon with $p_\mathrm{T} > 20$ GeV.

A dielectron control region in the 13 TeV data is defined using similar requirements on the two electrons as for the dimuon control region. Single-electron triggers with a p_T threshold of 27 GeV are used to record the events, and at least one of the selected electrons, after the full event reconstruction, is required to have $p_T > 40$ GeV. Additionally a single-photon trigger with a p_T threshold of 165 GeV is used to recover events in which the p_T of the Z boson is large (more than 600 GeV), leading to inefficiencies in the electron isolation requirements. A single-electron control sample is selected using the same triggers. The p_T of the electron in this region is required to be greater than 40 GeV in order to reach the region in which the trigger is fully efficient. An additional requirement of $E_T^{\text{miss}} > 50$ GeV is imposed on single-electron events in order to suppress the QCD multijet background.

The use of dilepton events to constrain the Z($\nu\nu$)+jets background suffers from large statistical uncertainties since the branching fraction of the Z boson to neutrinos is roughly six times larger than that to muons or electrons. In order to overcome this, γ+jets events are additionally used to reduce the statistical uncertainty at the cost of introducing theoretical uncertainties in their use for modelling Z($\nu\nu$)+jets events [78]. The γ+jets control sample is constructed using single-photon triggers. Events are required to have a well isolated photon with $p_T > 170$ (175) GeV and $|\eta| < 2.5$ (1.44) in the 8 (13) TeV analysis to ensure a γ+jets purity of at least 95% [33].

The events in all control regions are required to pass all of the selection requirements applied in the signal region, except for the lepton and photon vetoes. As in the signal region, events in the control regions are separated into V(jj) and monojet channels.

The E_T^{miss} distribution of the Z($\nu\nu$)+jets and W($\ell\nu$)+jets backgrounds is estimated from a maximum likelihood fit, performed simultaneously across all E_T^{miss} bins in the signal and control regions. The expected numbers of Z($\nu\nu$)+jets (and W($\ell\nu$)+jets in the 8 TeV analysis) in each bin of E_T^{miss} are free parameters of the fit. For each bin in E_T^{miss}, the ratio of the Z($\nu\nu$)+jets yield in the signal region to the corresponding yields of the Z($\mu^+\mu^-$)+jets, Z(e^+e^-)+jets and γ+jets processes in the dimuon, dielectron, and γ+jets control regions are used to determine the expectations in these control regions for given values of the fit parameters [61]. Similarly, the ratio of the W($\ell\nu$)+jets yield in the signal region to the corresponding yields of the W($\mu\nu$)+jets and W($e\nu$)+jets processes in the single-muon and single-electron control regions are used to determine the expectations in these two control regions. The ratios are determined from simulation after applying p_T-dependent NLO QCD K-factors derived using the MADGRAPH5_AMC@NLO2.2 MC generator and p_T-dependent NLO EW K-factors derived from theoretical calculations [79–82]. In the 8 TeV analysis, the ratio between the two backgrounds is left unconstrained in the fit. In the 13 TeV analysis, the ratio of W($\ell\nu$)+jets to Z($\nu\nu$)+jets in the signal region is constrained to that predicted in simulation after the application of NLO QCD and EW K-factors.

Systematic uncertainties are included to account for theoretical uncertainties in the γ to Z and W to Z differential cross section ratios due to the choice of the renormalisation and factorisation scales and uncertainties in the PDFs used to generate the events [83]. The value of the systematic uncertainty in these differential cross sections due to higher-order EW corrections is taken to be the full NLO EW correction, which can be as large as 20% for large values of E_T^{miss}. For the kinematic region in which the K-factors are applied,

the interference between QCD and EW effects reduces the correction obtained compared to applying the K-factors independently [82]. The difference between accounting for this interference or not is covered by the systematic uncertainties applied. Uncertainties in the selection efficiencies of muons, electrons, photons (up to 2%), and hadronically decaying τ leptons (3%) are included. The uncertainty in the modelling of $E_{\mathrm{T}}^{\mathrm{miss}}$ in simulation is dominated by the jet energy scale uncertainty and varies between 2 and 5%, depending on the $E_{\mathrm{T}}^{\mathrm{miss}}$ bin.

The remaining subdominant backgrounds due to top quark and diboson processes are estimated directly from simulation. Systematic uncertainties of 10 and 20% are included in the cross sections for the top quark [70] and diboson backgrounds [66, 67]. An additional 10% uncertainty is assigned to the top quark backgrounds to account for the discrepancies observed between data and the simulation in the p_{T} distribution of the $t\bar{t}$ pair. An inefficiency of the V(jj) tagging requirements can cause events to migrate between the V(jj) and monojet channels. An uncertainty in the V(jj) tagging efficiency of 13%, which allows for migration of events between the V(jj) and monojet channels, is included to account for this. This uncertainty comprises a statistical component which is uncorrelated between the 8 and 13 TeV analyses and a systematic component which is fully correlated.

In the 8 TeV data set, the contribution from QCD multijet events is determined using simulation normalised to the data, while in the 13 TeV data set the contribution is determined using a dedicated control sample. Although large uncertainties are included to account for the extrapolation from the control region to the signal region, the impact on the final results is small.

Figure 5 shows the distribution of $E_{\mathrm{T}}^{\mathrm{miss}}$ in data for the V(jj) and monojet channels in the 13 TeV analysis and the background predicted after performing a simultaneous fit, which ignores the constraints from data in the signal regions. The signal expectation assuming SM rates for production of a Higgs boson with a mass of 125 GeV with $\mathcal{B}(\mathrm{H} \to \mathrm{inv}) = 100\%$ is superimposed.

5 Results

No significant deviations from the SM expectations are observed in any of the searches performed. The results are interpreted in terms of upper limits on $\mathcal{B}(\mathrm{H} \to \mathrm{inv})$ under various assumptions about the Higgs boson production cross section, σ. Limits are calculated using an asymptotic approximation of the CL$_{\mathrm{s}}$ prescription [84, 85] using a profile likelihood ratio test statistic [86], in which systematic uncertainties are modelled as nuisance parameters $\boldsymbol{\theta}$ following a frequentist approach [87].

The profile likelihood ratio is defined as,

$$q = -2 \ln \frac{L(\mathrm{data} | \sigma \, \mathcal{B}(\mathrm{H} \to \mathrm{inv})/\sigma(\mathrm{SM}), \hat{\hat{\boldsymbol{\theta}}})}{L(\mathrm{data} | \sigma \, \hat{\mathcal{B}}(\mathrm{H} \to \mathrm{inv})/\sigma(\mathrm{SM}), \hat{\boldsymbol{\theta}})},$$

where $\sigma \, \hat{\mathcal{B}}(\mathrm{H} \to \mathrm{inv})/\sigma(\mathrm{SM})$ represents the value of $\sigma \, \mathcal{B}(\mathrm{H} \to \mathrm{inv})/\sigma(\mathrm{SM})$, which maximises the likelihood L for the data, and $\hat{\boldsymbol{\theta}}$ and $\hat{\hat{\boldsymbol{\theta}}}$ denote the unconditional maximum
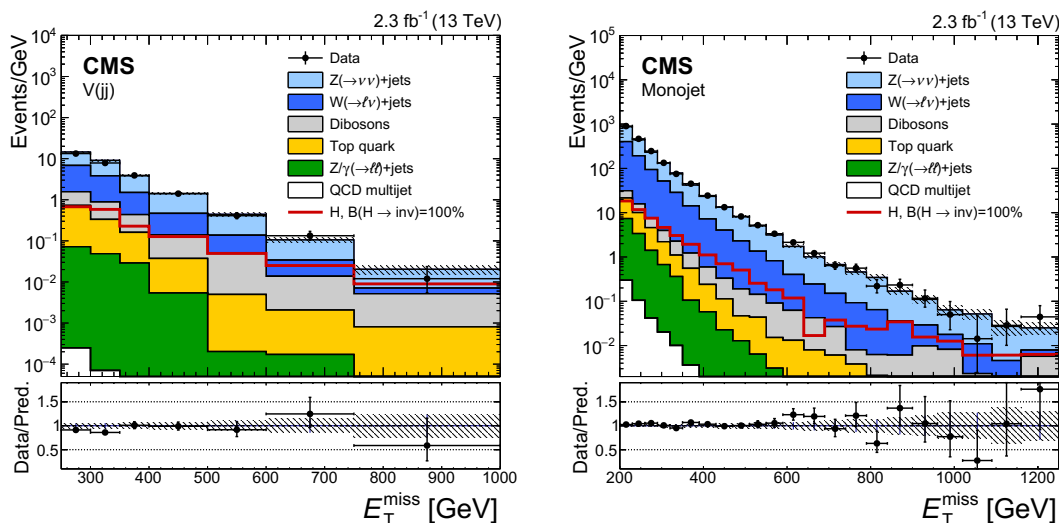
Figure 5. Distributions of E_T^{miss} in data and predicted background contributions in the (left) V(jj) and (right) monojet channels at 13 TeV. The background prediction is taken from a fit using only the control regions and the shaded bands represent the statistical and systematic uncertainties in the backgrounds after that fit. The horizontal bars on the data points represent the width of the bin centred at that point. The expectations from a Higgs boson with a mass of 125 GeV decaying to invisible particles with a branching fraction of 100% are superimposed.

likelihood estimates for the nuisance parameters and the estimates for a specific value of $\sigma \mathcal{B}(H \to inv)/\sigma(SM)$. The value of $\sigma \mathcal{B}(H \to inv)/\sigma(SM)$ is restricted to be positive when maximising the likelihood. The "data" here refers to the data in all of the control and signal regions for each analysis described in section 4.

The statistical procedure accounts for correlations between the nuisance parameters in each of the analyses. The uncertainties in the diboson cross sections, the lepton efficiencies, momentum scales, and the integrated luminosity are correlated across all categories of a given data set. The uncertainties in the inclusive signal cross sections are additionally correlated across the measurements at 7, 8, and 13 TeV.

The kinematics of the jets selected in the VBF channel are distinct from those selected in the V(jj) and monojet channels. For this reason, the jet energy scale and resolution uncertainties are considered uncorrelated between those channels. The b jet energy scale and resolution uncertainties for the Z(b$\bar{\text{b}}$) channel are estimated using a different technique from that used for other jets and so are treated as uncorrelated with other searches [88].

Where simulation is used to model the E_T^{miss} distributions of the signal or backgrounds, uncertainties are propagated from the jet and lepton energy scales and resolutions as well as from modelling of the unclustered energy. These uncertainties are treated as fully correlated between the 7, 8, and 13 TeV data sets, except for the 8 TeV V(jj) and monojet channels for which independent calibrations based on control samples in data are applied.

Systematic uncertainties in the inclusive ggH, qqH, and VH production cross sections due to renormalisation and factorisation scales, and PDF uncertainties are taken directly from ref. [51] and treated as fully correlated across the 7, 8, and 13 TeV data sets. An
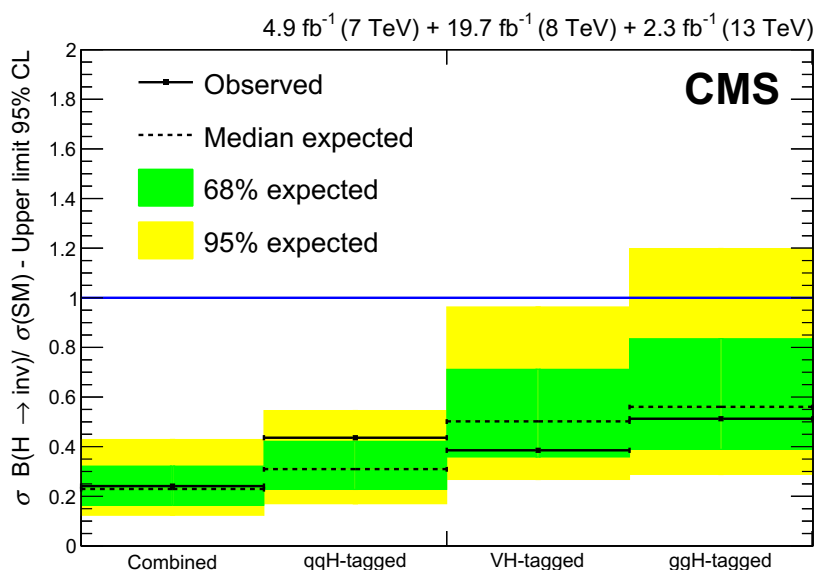
Figure 6. Observed and expected 95% CL limits on $\sigma \mathcal{B}(\mathrm{H} \to \mathrm{inv})/\sigma(\mathrm{SM})$ for individual combinations of categories targeting qqH, VH, and ggH production, and the full combination assuming a Higgs boson with a mass of 125 GeV.

additional systematic uncertainty of 50% in the ggH production cross section of the Higgs boson in association with two jets is included for the contribution of ggH production in the VBF categories. This uncertainty is estimated by comparing the two-jet NLO generators POWHEG 2.0+MINLO [89] and aMC@NLO [90] interfaced with HERWIG++ 2.3 [91]. Furthermore, an uncertainty in the Higgs boson p_T distribution in ggH production is included in the monojet channels and estimated by varying the renormalisation and factorisation scales [92]. This uncertainty is correlated between the 8 and 13 TeV categories. Uncertainties in the acceptance arising from uncertainties in the PDFs used to determine the expected signal yields are evaluated independently for the different signal processes in each event category and treated as additional normalisation nuisance parameters.

5.1 Upper limits on $\mathcal{B}(\mathrm{H} \to \mathrm{inv})$ assuming SM production

Observed and expected upper limits on $\sigma \mathcal{B}(\mathrm{H} \to \mathrm{inv})/\sigma(\mathrm{SM})$, where $\sigma(\mathrm{SM})$ is the total SM Higgs boson production cross section, are determined at the 95% CL and presented in figure 6. The limits are obtained from the combination of all categories and from sub-combinations of categories, which target one of the ggH, qqH, and VH production mechanisms, corresponding to the analysis tags in table 2. The relative contributions from the different production mechanisms in these results are fixed to their SM predictions within the uncertainties. If the production cross sections take their SM values, the results can be used to constrain the branching fraction of the Higgs boson to invisible particles. Assuming SM production rates for the ggH, qqH, and VH modes, the combination yields an observed (expected) upper limit of $\mathcal{B}(\mathrm{H} \to \mathrm{inv}) < 0.24$ (0.23) at the 95% CL.
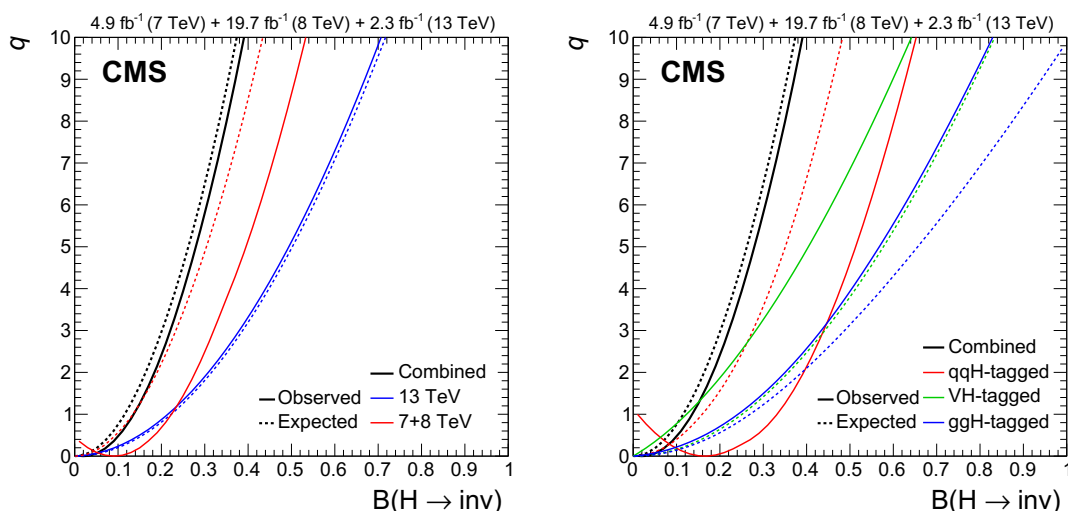
Figure 7. Profile likelihood ratio as a function of $\mathcal{B}(\text{H} \to \text{inv})$ assuming SM production cross sections of a Higgs boson with a mass of 125 GeV. The solid curves represent the observations in data and the dashed curves represent the expected result assuming no invisible decays of the Higgs boson. (left) The observed and expected likelihood scans for the partial combinations of the 7+8 and 13 TeV analyses, and the full combination. (right) The observed and expected likelihood scans for the partial combinations of the qqH-tagged, VH-tagged, and ggH-tagged analyses, and the full combination.

The profile likelihood ratios as a function of $\mathcal{B}(\text{H} \to \text{inv})$ using partial combinations of the 7+8 and 13 TeV analyses, and for the full combination are shown in figure 7 (left). The profile likelihood ratio scans for the partial combinations of the qqH-tagged, VH-tagged, and ggH-tagged analyses are shown in figure 7 (right). The results are shown for the data and for an Asimov data set, defined as the data set for which the maximum likelihood estimates of all parameters are equal to their true values [86], in which $\mathcal{B}(\text{H} \to \text{inv}) = 0$ is assumed.

The dominant systematic uncertainties for the qqH-tagged, $\text{Z}(\ell^+\ell^-)$, V(jj), and ggH-tagged searches in the 13 TeV data set are listed in tables 8, 9, 10, and 11, respectively.

The impact of each independent source of systematic uncertainty is calculated for an Asimov data set in which $\sigma \mathcal{B}(\text{H} \to \text{inv})/\sigma(\text{SM})$ is assumed to be 1. The impact is defined as the maximum difference in the fitted value of $\sigma \mathcal{B}(\text{H} \to \text{inv})/\sigma(\text{SM})$, when varying the nuisance parameter associated to that source of systematic uncertainty within one standard deviation of its maximum likelihood estimate. The total systematic uncertainty, and the total uncertainty fixing all nuisance parameters associated to systematic uncertainties that are not expected to improve with additional luminosity (statistical only), for each analysis is also shown. Finally, the total uncertainty is given for each analysis. The statistical only and total uncertainties are determined from the interval in $\sigma \mathcal{B}(\text{H} \to \text{inv})/\sigma(\text{SM})$ for which $q < 1$. The total systematic uncertainty is determined by subtracting the statistical only uncertainty from the total uncertainty in quadrature. With the luminosity of the 13 TeV data set, the sensitivity of the qqH-tagged and $\text{Z}(\ell^+\ell^-)$ analyses is dominated by

Systematic uncertainty	Impact
Common	
W to Z ratio in QCD produced V+jets	13%
W to Z ratio in EW produced V+jets	6.3%
Jet energy scale and resolution	6.0%
QCD multijet normalisation	4.3%
Pileup mismodelling	4.2%
Lepton efficiencies	2.5%
Integrated luminosity	2.2%
Signal specific	
ggH acceptance	3.8%
Renorm. and fact. scales and PDF (qqH)	1.8%
Renorm. and fact. scales and PDF (ggH)	<0.2%
Total systematic	$^{+15}_{-19}$%
Total statistical only	$^{+28}_{-27}$%
Total uncertainty	$^{+32}_{-33}$%

Table 8. Dominant sources of systematic uncertainties and their impact on the fitted value of $\mathcal{B}(\mathrm{H} \to \mathrm{inv})$ in the VBF analysis at 13 TeV. The systematic uncertainties are split into common uncertainties and those specific to the signal model. The total systematic uncertainty, the total uncertainty fixing all constrained nuisance parameters to their maximum likelihood estimates (statistical only), and the total uncertainty are also given.

the statistical uncertainty while for the V(jj) and ggH-tagged analyses, a reduction in the theoretical and experimental systematic uncertainties related to the modelling of the $\mathrm{Z}(\nu\nu)$+jets and $\mathrm{W}(\ell\nu)$+jets backgrounds would yield significant improvements.

5.2 Non-SM production and DM interpretations

By varying the assumed SM production rates, the relative sensitivity of the different categories to an invisible Higgs boson decay signal is studied. The rates for ggH, qqH, and VH production can be expressed in terms of the relative coupling modifiers κ_F and κ_V that scale the couplings of the Higgs boson to the SM fermions and vector bosons, respectively [47]. In this formalism, the total width of the Higgs boson is the sum of the partial widths to the visible channels, determined as a function of κ_V and κ_F, and an invisible decay width. The contribution from the gg $\to$ ZH mode is scaled to account for the interference between the tH and ZH diagrams (see figure 2). The background from $\mathrm{Z}(\nu\nu)\mathrm{H}(\mathrm{b\bar{b}})$ production in the $\mathrm{Z}(\mathrm{b\bar{b}})$ search is scaled consistently with the other search channels. The SM production rates are recovered for $\kappa_F = \kappa_V = 1$. Figure 8 shows 95% CL upper limits on $\mathcal{B}(\mathrm{H} \to \mathrm{inv})$ obtained as a function of κ_F and κ_V. The best-fit, and 68 and 95% CL limits for κ_F, κ_V from ref. [4] are superimposed. The observed upper limit on $\mathcal{B}(\mathrm{H} \to \mathrm{inv})$

Systematic uncertainty	Impact
Common	
ZZ background, theory	16%
Integrated luminosity	8.4%
b tagging efficiency	6.2%
Electron efficiency	6.2%
Muon efficiency	6.2%
Electron energy scale	3.2%
Muon momentum scale	3.2%
Jet energy scale	2.2%
Diboson normalisation	5.3%
$e\mu$ region extrapolation	4.0%
$Z(\ell^+\ell^-)$ normalisation	4.8%
Signal specific	
Renorm. and fact. scales and PDF (qqZH)	7.4%
Renorm. and fact. scales and PDF (ggZH)	4.0%
Total systematic	$^{+27}_{-23}$%
Total statistical only	$^{+56}_{-50}$%
Total uncertainty	$^{+62}_{-55}$%

Table 9. Dominant sources of systematic uncertainties and their impact on the fitted value of $\mathcal{B}(\mathrm{H} \to \mathrm{inv})$ in the $Z(\ell^+\ell^-)$ analysis at 13 TeV. The systematic uncertainties are split into common uncertainties and those specific to the signal model. The total systematic uncertainty, the total uncertainty fixing all constrained nuisance parameters to their maximum likelihood estimates (statistical only), and the total uncertainty are also given.

varies between 0.18 and 0.29 within the 95% confidence level region shown. An alternative model under which the production rates are varied is described in appendix A.

The upper limit on $\mathcal{B}(\mathrm{H} \to \mathrm{inv})$, under the assumption of SM production cross sections for the Higgs boson, can be interpreted in the context of a Higgs-portal model of DM interactions. In these models, a hidden sector provides a stable DM particle candidate with tree-level couplings to the SM Higgs sector. Direct detection experiments are sensitive to elastic interactions between DM particles and nuclei via Higgs boson exchange. These interactions produce nuclear recoil signatures, which can be interpreted in terms of a DM-nucleon interaction cross section. The sensitivity varies as a function of the DM particle mass m_χ with relatively small DM masses being harder to probe. If the DM mass is smaller than $m_\mathrm{H}/2$, the invisible Higgs boson decay width, Γ_inv, can be translated via an effective field theory approach into the spin-independent DM-nucleon elastic cross section σ^SI, assuming either a scalar or fermion DM candidate [10]. The translation is given by

$$\sigma^\mathrm{SI}_\mathrm{S-N} = \frac{4\Gamma_\mathrm{inv}}{m_\mathrm{H}^3 v^2 \beta} \frac{m_\mathrm{N}^4 f_\mathrm{N}^2}{(m_\chi + m_\mathrm{N})^2}, \tag{5.1}$$

Systematic uncertainty	Impact
Common	
γ+jets/Z($\nu\nu$)+jets ratio, theory	32%
W($\ell\nu$)+jets/Z($\nu\nu$)+jets ratio, theory	21%
Jet energy scale and resolution	12%
V(jj)-tagging efficiency	12%
Lepton veto efficiency	13%
Electron efficiency	13%
Muon efficiency	8.6%
b tagging efficiency	5.7%
Photon efficiency	3.1%
$E_{\mathrm{T}}^{\mathrm{miss}}$ scale	4.6%
Top quark background normalisation	6.0%
Diboson background normalisation	<1%
Integrated luminosity	<1%
Signal specific	
ggH p_{T}-spectrum	12%
Renorm. and fact. scales and PDF (ggH)	3.0%
Renorm. and fact. scales and PDF (VH)	1.4%
Total systematic	$^{+55}_{-51}$%
Total statistical only	$^{+50}_{-46}$%
Total uncertainty	$^{+74}_{-69}$%

Table 10. Dominant sources of systematic uncertainties and their impact on the fitted value of $\mathcal{B}(\mathrm{H} \to \mathrm{inv})$ in the V(jj)analysis at 13 TeV. The systematic uncertainties are split into common uncertainties and those specific to the signal model. The total systematic uncertainty, the total uncertainty fixing all constrained nuisance parameters to their maximum likelihood estimates (statistical only), and the total uncertainty are also given.

assuming a scalar DM candidate, and

$$\sigma_{\mathrm{f-N}}^{\mathrm{SI}} = \frac{8\Gamma_{\mathrm{inv}} m_\chi^2}{m_{\mathrm{H}}^5 v^2 \beta^3} \frac{m_{\mathrm{N}}^4 f_{\mathrm{N}}^2}{(m_\chi + m_{\mathrm{N}})^2}, \tag{5.2}$$

assuming a fermion DM candidate, where m_{N} is the average of the proton and neutron masses 0.939 GeV and $\beta = \sqrt{1 - 4m_\chi^2/m_{\mathrm{H}}^2}$. The Higgs vacuum expectation value v is taken to be 246 GeV. The dimensionless quantity f_{N} denotes the nuclear form-factor. The central values for the exclusion limits are derived assuming $f_{\mathrm{N}} = 0.326$, taken from ref. [93], while alternative values of 0.260 and 0.629 are taken from the MILC Collaboration [94]. The translation between Γ_{inv} and $\mathcal{B}(\mathrm{H} \to \mathrm{inv})$ uses the relation $\mathcal{B}(\mathrm{H} \to \mathrm{inv}) = \Gamma_{\mathrm{inv}}/(\Gamma_{\mathrm{SM}} + \Gamma_{\mathrm{inv}})$, where $\Gamma_{\mathrm{SM}} = 4.07$ MeV [47]. Figure 9 shows the 90% CL upper limits on the spin-independent DM-nucleon cross section as a function of the DM mass, assuming $m_{\mathrm{H}} = 125$ GeV, for the scalar and fermion DM scenarios. These limits are calculated using the 90%

Systematic uncertainty	Impact
Common	
Muon efficiency	24%
Electron efficiency	22%
Lepton veto efficiency	16%
b jet tag efficiency	3.2%
$W(\ell\nu)$+jets/$Z(\nu\nu)$+jets ratio, theory	16%
γ+jets/$Z(\nu\nu)$+jets ratio, theory	5.8%
Jet energy scale and resolution	10%
E_T^{miss} scale	1.8%
Integrated luminosity	3.0%
Diboson background normalisation	2.7%
Top quark background normalisation	<1%
Signal specific	
ggH p_T-spectrum	15%
Renorm. and fact. scales and PDF (ggH)	5.8%
Total systematic	$^{+57}_{-50}$%
Total statistical only	$^{+25}_{-22}$%
Total uncertainty	$^{+62}_{-55}$%

Table 11. Dominant sources of systematic uncertainties and their impact on the fitted value of $\mathcal{B}(H \to inv)$ in the monojet analysis at 13 TeV. The systematic uncertainties are split into common uncertainties and those specific to the signal model. The total systematic uncertainty, the total uncertainty fixing all constrained nuisance parameters to their maximum likelihood estimates (statistical only), and the total uncertainty are also given.

CL limit of $\mathcal{B}(H \to inv) < 0.20$ in order to compare with those from the LUX [95], PandaX-II [96], and CDMSlite [97] experiments, which provide the strongest direct constraints on the spin-independent DM-nucleon cross section in the range of DM particle masses probed by this analysis. Under the assumptions of the Higgs-portal models, the present CMS results provide more stringent limits for DM masses below roughly 20 or 5 GeV, assuming a fermion or scalar DM particle, respectively.

6 Summary

A combination of searches for a Higgs boson decaying to invisible particles using proton-proton collision data collected during 2011, 2012, and 2015, at centre-of-mass energies of 7, 8, and 13 TeV, respectively, is presented. The combination includes searches targeting Higgs boson production in the ZH mode, in which a Z boson decays to $\ell^+\ell^-$ or $b\bar{b}$, and the qqH mode, which is the most sensitive channel. The combination also includes the first searches at CMS targeting VH production, in which the vector boson decays hadronically, and the ggH mode in which the Higgs boson is produced in association with jets. No
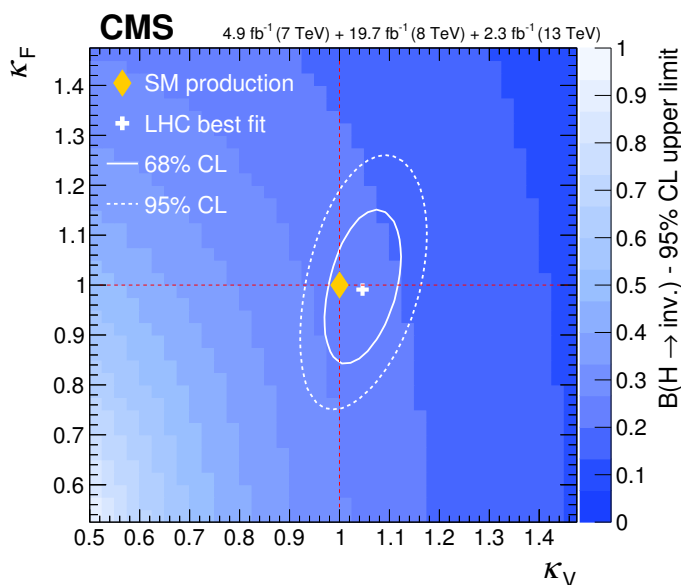
Figure 8. Observed 95% CL upper limits on $\mathcal{B}(H \to \text{inv})$ assuming a Higgs boson with a mass of 125 GeV whose production cross sections are scaled, relative to their SM values as a function of the coupling modifiers κ_F and κ_V. The best-fit, and 68 and 95% confidence level regions for κ_F and κ_V from ref. [4] are superimposed as the solid and dashed white contours, respectively. The SM prediction (yellow diamond) corresponds to $\kappa_F = \kappa_V = 1$.
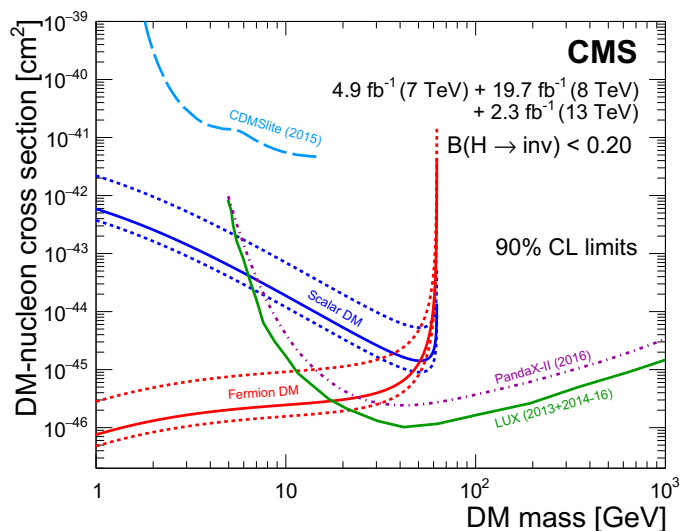
Figure 9. Limits on the spin-independent DM-nucleon scattering cross section in Higgs-portal models assuming a scalar or fermion DM particle. The dashed lines show the variation in the exclusion limit using alternative values for f_N as described in the text. The limits are given at the 90% CL to allow for comparison to direct detection constraints from the LUX [95], PandaX-II [96], and CDMSlite [97] experiments.

significant deviations from the SM predictions are observed and upper limits are placed on the branching fraction for the Higgs boson decay to invisible particles. The combination of all searches yields an observed (expected) upper limit on $\mathcal{B}(\text{H} \to \text{inv})$ of 0.24 (0.23) at the 95% confidence level, assuming SM production of the Higgs boson. The combined 90% confidence level limit of $\mathcal{B}(\text{H} \to \text{inv}) < 0.20$ has been interpreted in Higgs-portal models and constraints are placed on the spin-independent DM-nucleon interaction cross section. These limits provide stronger constraints than those from direct detection experiments for DM masses below roughly $20\,(5)\,\text{GeV}$, assuming a fermion (scalar) DM particle, within the context of Higgs-portal models.

Acknowledgments

A   Supplementary material

A.1   Negative likelihood scans

The profile likelihood ratio as a function of $\mathcal{B}(\mathrm{H} \to \mathrm{inv})$ using partial combinations of the 7+8 and 13 TeV analyses, and for the full combination are shown in figure 10 (left). The profile likelihood ratio scans for the partial combinations of the VBF-tagged, VH-tagged, and ggH-tagged analyses are shown in figure 10 (right). The results are shown for the data and for an Asimov data set [86] in which $\mathcal{B}(\mathrm{H} \to \mathrm{inv}) = 0$ is assumed. For these results, the condition that $\mathcal{B}(\mathrm{H} \to \mathrm{inv}) > 0$ is removed.
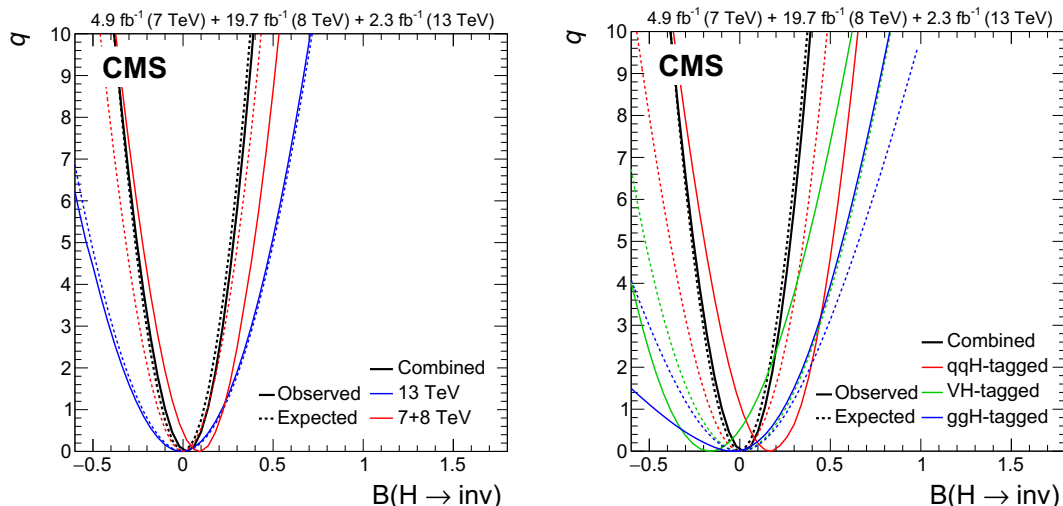
Figure 10. Profile likelihood ratio as a function of $\mathcal{B}(\mathrm{H} \to \mathrm{inv})$ assuming SM production cross sections of a Higgs boson with a mass of 125 GeV. The solid curves represent the observations in data and the dashed curves represent the expected result assuming no invisible decays of the Higgs boson. (left) The observed and expected likelihood scans for the partial combinations of the 7+8 and 13 TeV analyses, and the full combination. (right) The observed and expected likelihood scans for the partial combinations of the VBF-tagged, VH-tagged, and ggH-tagged analyses, and the full combination.
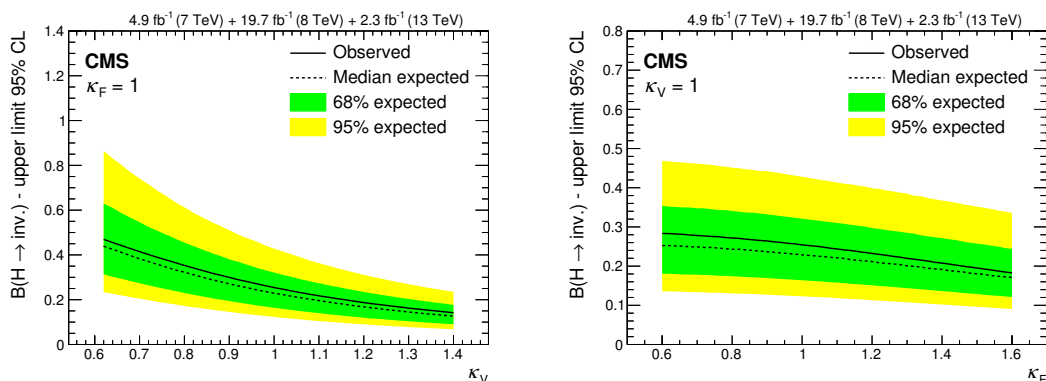

Figure 11. Observed and expected 95% CL upper limits on $\mathcal{B}(\mathrm{H} \to \mathrm{inv})$ assuming a Higgs boson with a mass of 125 GeV whose production cross sections are scaled, relative to their SM values as a function of (left) κ_V, fixing $\kappa_F = 1$ and (right) κ_F, fixing $\kappa_V = 1$.

A.2 Non-SM production cross sections

Figure 11 shows the observed and expected 95% CL upper limits on $\mathcal{B}(\mathrm{H} \to \mathrm{inv})$ obtained as a function of either κ_V, fixing $\kappa_F = 1$ or as a function of κ_F, fixing $\kappa_V = 1$.

The rates for the different production modes can be scaled by the multiplicative factors μ_{ggH} and $\mu_{\mathrm{qqH,VH}}$ which respectively denote the production cross section values for the ggH and qqH/VH modes relative to their SM predictions. The SM production cross sections are therefore attained for $\mu_{\mathrm{ggH}} = \mu_{\mathrm{qqH,VH}} = 1$. Figure 12 shows the 95% CL upper limits on $\mathcal{B}(\mathrm{H} \to \mathrm{inv})$ obtained as a function of μ_{ggH} and $\mu_{\mathrm{qqH,VH}}$.
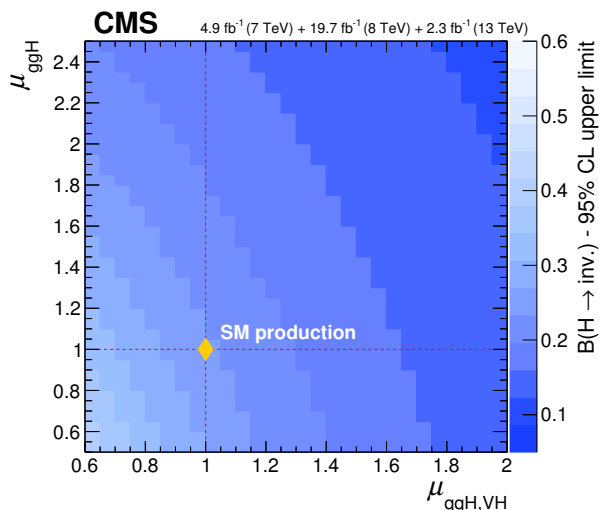
Figure 12. Observed 95% CL upper limits on $\mathcal{B}(H \to \text{inv})$ assuming a Higgs boson with a mass of 125 GeV whose production cross sections are scaled, relative to their SM values, by μ_{ggH} and $\mu_{\text{qqH,VH}}$. The SM (yellow diamond) is attained for $\mu_{\text{ggH}} = \mu_{\text{qqH,VH}} = 1$.
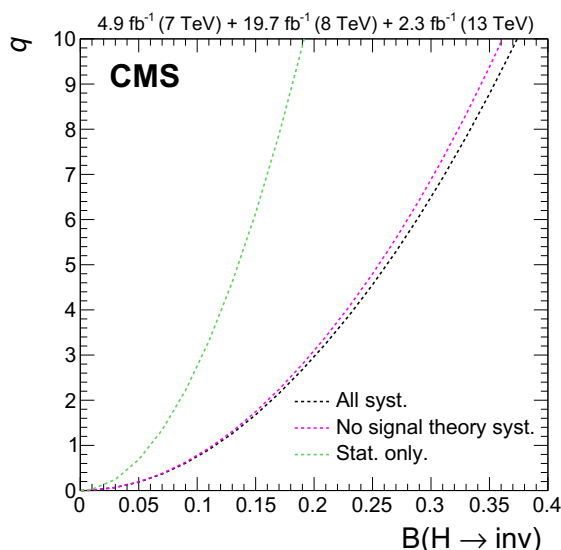

Figure 13. Expected profile likelihood ratio as a function of $\mathcal{B}(H \to \text{inv})$ assuming SM production cross sections of a Higgs boson with a mass of 125 GeV. The results fixing all nuisance parameters associated to theoretical systematic uncertainties on the signal to their nominal values in data is shown as the magenta line. The result assuming only statistical uncertainties is also shown in green.

A.3 Uncertainty breakdown

The profile likelihood ratio using the Asimov dataset fixing all nuisance parameters associated with theoretical systematic uncertainties in the signal model to their nominal values from the combined fit to data is shown in figure 13. A second result including only statistical uncertainties is additionally shown.

References

[1] ATLAS collaboration, *Observation of a new particle in the search for the Standard Model Higgs boson with the ATLAS detector at the LHC*, *Phys. Lett.* **B 716** (2012) 1 [`arXiv:1207.7214`] [INSPIRE].

[2] CMS collaboration, *Observation of a new boson at a mass of 125 GeV with the CMS experiment at the LHC*, *Phys. Lett.* **B 716** (2012) 30 [`arXiv:1207.7235`] [INSPIRE].

[3] CMS collaboration, *Observation of a new boson with mass near 125 GeV in pp collisions at $\sqrt{s} = 7$ and 8 TeV*, *JHEP* **06** (2013) 081 [`arXiv:1303.4571`] [INSPIRE].

[4] ATLAS and CMS collaborations, *Measurements of the Higgs boson production and decay rates and constraints on its couplings from a combined ATLAS and CMS analysis of the LHC pp collision data at $\sqrt{s} = 7$ and 8 TeV*, *JHEP* **08** (2016) 045 [`arXiv:1606.02266`] [INSPIRE].

[5] G. Bélanger, F. Boudjema, A. Cottrant, R.M. Godbole and A. Semenov, *The MSSM invisible Higgs in the light of dark matter and g-2*, *Phys. Lett.* **B 519** (2001) 93 [`hep-ph/0106275`] [INSPIRE].

[6] G.F. Giudice, R. Rattazzi and J.D. Wells, *Graviscalars from higher dimensional metrics and curvature Higgs mixing*, *Nucl. Phys.* **B 595** (2001) 250 [`hep-ph/0002178`] [INSPIRE].

[7] D. Dominici and J.F. Gunion, *Invisible Higgs decays from Higgs-graviscalar mixing*, *Phys. Rev.* **D 80** (2009) 115006 [`arXiv:0902.1512`] [INSPIRE].

[8] R.E. Shrock and M. Suzuki, *Invisible decays of Higgs bosons*, *Phy. Lett.* **B 110** (1982) 250.

[9] S. Baek, P. Ko, W.-I. Park and E. Senaha, *Higgs portal vector dark matter: revisited*, *JHEP* **05** (2013) 036 [`arXiv:1212.2131`] [INSPIRE].

[10] A. Djouadi, O. Lebedev, Y. Mambrini and J. Quevillon, *Implications of LHC searches for Higgs-portal dark matter*, *Phys. Lett.* **B 709** (2012) 65 [`arXiv:1112.3299`] [INSPIRE].

[11] A. Djouadi, A. Falkowski, Y. Mambrini and J. Quevillon, *Direct detection of Higgs-portal dark matter at the LHC*, *Eur. Phys. J.* **C 73** (2013) 2455 [`arXiv:1205.3169`] [INSPIRE].

[12] A. Beniwal et al., *Combined analysis of effective Higgs portal dark matter models*, *Phys. Rev.* **D 93** (2016) 115016 [`arXiv:1512.06458`] [INSPIRE].

[13] G. Servant and S. Tulin, *Baryogenesis and dark matter through a Higgs asymmetry*, *Phys. Rev. Lett.* **111** (2013) 151601 [`arXiv:1304.3464`] [INSPIRE].

[14] T. Cohen, D.E. Morrissey and A. Pierce, *Electroweak baryogenesis and Higgs signatures*, *Phys. Rev.* **D 86** (2012) 013009 [`arXiv:1203.2924`] [INSPIRE].

[15] ATLAS collaboration, *Search for invisible decays of a Higgs boson produced in association with a Z boson in ATLAS*, *Phys. Rev. Lett.* **112** (2014) 201802 [`arXiv:1402.3244`] [INSPIRE].

[16] ATLAS collaboration, *Search for invisible decays of the Higgs boson produced in association with a hadronically decaying vector boson in pp collisions at $\sqrt{s} = 8$ TeV with the ATLAS detector*, *Eur. Phys. J.* **C 75** (2015) 337 [`arXiv:1504.04324`] [INSPIRE].

[17] CMS collaboration, *Search for invisible decays of Higgs bosons in the vector boson fusion and associated ZH production modes*, *Eur. Phys. J.* **C 74** (2014) 2980 [`arXiv:1404.1344`] [INSPIRE].

[18] ATLAS collaboration, *Search for invisible decays of a Higgs boson using vector-boson fusion in pp collisions at $\sqrt{s} = 8\ TeV$ with the ATLAS detector*, *JHEP* **01** (2016) 172 [arXiv:1508.07869] [INSPIRE].

[19] ATLAS collaboration, *Constraints on new phenomena via Higgs boson couplings and invisible decays with the ATLAS detector*, *JHEP* **11** (2015) 206 [arXiv:1509.00672] [INSPIRE].

[20] ATLAS collaboration, *Search for new phenomena in final states with an energetic jet and large missing transverse momentum in pp collisions at $\sqrt{s} = 8\ TeV$ with the ATLAS detector*, *Eur. Phys. J.* **C 75** (2015) 299 [*Erratum ibid.* **75** (2015) 408] [arXiv:1502.01518] [INSPIRE].

[21] CMS collaboration, *The CMS experiment at the CERN LHC*, 2008 *JINST* **3** S08004 [INSPIRE].

[22] CMS collaboration, *Particle-flow event reconstruction in CMS and performance for jets, taus and MET*, CMS-PAS-PFT-09-001 (2009).

[23] CMS collaboration, *Commissioning of the particle-flow event reconstruction with the first LHC collisions recorded in the CMS detector*, CMS-PAS-PFT-10-001 (2010).

[24] M. Cacciari, G.P. Salam and G. Soyez, *The anti-k_t jet clustering algorithm*, *JHEP* **04** (2008) 063 [arXiv:0802.1189] [INSPIRE].

[25] CMS collaboration, *A Cambridge-Aachen (C-A) based jet algorithm for boosted top-jet tagging*, CMS-PAS-JME-09-001 (2009).

[26] CMS collaboration, *Identification of b-quark jets with the CMS experiment*, 2013 *JINST* **8** P04013 [arXiv:1211.4462] [INSPIRE].

[27] CMS collaboration, *Performance of b tagging at $\sqrt{s} = 8\ TeV$ in multijet, ttbar and boosted topology events*, CMS-PAS-BTV-13-001 (2013).

[28] CMS collaboration, *Identification of b quark jets at the CMS Experiment in the LHC Run 2*, CMS-PAS-BTV-15-001 (2016).

[29] M. Cacciari, G.P. Salam and G. Soyez, *FastJet user manual*, *Eur. Phys. J.* **C 72** (2012) 1896 [arXiv:1111.6097] [INSPIRE].

[30] CMS collaboration, *Jet energy scale and resolution in the CMS experiment in pp collisions at 8 TeV*, [arXiv:1607.03663] [INSPIRE].

[31] CMS collaboration, *Determination of Jet Energy Calibration and Transverse Momentum Resolution in CMS*, 2011 *JINST* **6** P11002 [arXiv:1107.4277] [INSPIRE].

[32] CMS collaboration, *Performance of Electron Reconstruction and Selection with the CMS Detector in Proton-Proton Collisions at $\sqrt{s} = 8\ TeV$*, 2015 *JINST* **10** P06005 [arXiv:1502.02701] [INSPIRE].

[33] CMS collaboration, *Performance of Photon Reconstruction and Identification with the CMS Detector in Proton-Proton Collisions at $\sqrt{s} = 8\ TeV$*, 2015 *JINST* **10** P08010 [arXiv:1502.02702] [INSPIRE].

[34] CMS collaboration, *Performance of CMS muon reconstruction in pp collision events at $\sqrt{s} = 7\ TeV$*, 2012 *JINST* **7** P10002 [arXiv:1206.4071] [INSPIRE].

[35] M. Cacciari and G.P. Salam, *Pileup subtraction using jet areas*, *Phys. Lett.* **B 659** (2008) 119 [arXiv:0707.1378] [INSPIRE].

[36] CMS collaboration, *Reconstruction and identification of τ lepton decays to hadrons and ν_τ at CMS*, 2016 *JINST* **11** P01019 [arXiv:1510.07488] [INSPIRE].

[37] CMS collaboration, *The performance of the CMS muon detector in proton-proton collisions at $\sqrt{s} = 7\,TeV$ at the LHC*, 2013 *JINST* **8** P11002 [arXiv:1306.6905] [INSPIRE].

[38] CMS collaboration, *Absolute calibration of the luminosity measurement at CMS: Winter 2012 Update*, CMS-PAS-SMP-12-008 (2012).

[39] CMS collaboration, *CMS Luminosity Based on Pixel Cluster Counting - Summer 2013 Update*, CMS-PAS-LUM-13-001 (2013).

[40] CMS collaboration, *CMS luminosity measurement for the 2015 data-taking period*, CMS-PAS-LUM-15-001 (2015).

[41] S. Alioli, P. Nason, C. Oleari and E. Re, *A general framework for implementing NLO calculations in shower Monte Carlo programs: the POWHEG BOX*, *JHEP* **06** (2010) 043 [arXiv:1002.2581] [INSPIRE].

[42] P. Nason and C. Oleari, *NLO Higgs boson production via vector-boson fusion matched with shower in POWHEG*, *JHEP* **02** (2010) 037 [arXiv:0911.5299] [INSPIRE].

[43] S. Alioli, P. Nason, C. Oleari and E. Re, *NLO Higgs boson production via gluon fusion matched with shower in POWHEG*, *JHEP* **04** (2009) 002 [arXiv:0812.0578] [INSPIRE].

[44] T. Sjöstrand, S. Mrenna and P.Z. Skands, *PYTHIA 6.4 physics and manual*, *JHEP* **05** (2006) 026 [hep-ph/0603175] [INSPIRE].

[45] T. Sjöstrand, S. Mrenna and P.Z. Skands, *A brief introduction to PYTHIA 8.1*, *Comput. Phys. Commun.* **178** (2008) 852 [arXiv:0710.3820] [INSPIRE].

[46] C. Anastasiou et al., *Higgs boson gluon-fusion production at threshold in N^3LO QCD*, *Phys. Lett.* **B 737** (2014) 325 [arXiv:1403.4616] [INSPIRE].

[47] LHC Higgs Cross section Working Group collaboration, J.R. Andersen et al., *Handbook of LHC Higgs cross sections: 3. Higgs properties*, arXiv:1307.1347 [INSPIRE].

[48] D. de Florian, G. Ferrera, M. Grazzini and D. Tommasini, *Higgs boson production at the LHC: transverse momentum resummation effects in the $H \to \gamma\gamma$, $H \to WW \to l\nu l\nu$ and $H \to ZZ \to 4l$ decay modes*, *JHEP* **06** (2012) 132 [arXiv:1203.6321] [INSPIRE].

[49] M. Grazzini and H. Sargsyan, *Heavy-quark mass effects in Higgs boson production at the LHC*, *JHEP* **09** (2013) 129 [arXiv:1306.4581] [INSPIRE].

[50] ATLAS and CMS collaborations, *Combined measurement of the Higgs boson mass in pp collisions at $\sqrt{s} = 7$ and $8\,TeV$ with the ATLAS and CMS experiments*, *Phys. Rev. Lett.* **114** (2015) 191803 [arXiv:1503.07589] [INSPIRE].

[51] LHC Higgs Cross section Working Group collaboration, D. de Florian et al., *Handbook of LHC higgs cross sections: 4. Deciphering the nature of the Higgs sector*, arXiv:1610.07922 [INSPIRE].

[52] J. Alwall, M. Herquet, F. Maltoni, O. Mattelaer and T. Stelzer, *MadGraph 5: going beyond*, *JHEP* **06** (2011) 128 [arXiv:1106.0522] [INSPIRE].

[53] J. Alwall et al., *The automated computation of tree-level and next-to-leading order differential cross sections and their matching to parton shower simulations*, *JHEP* **07** (2014) 079 [arXiv:1405.0301] [INSPIRE].

[54] S. Alioli, P. Nason, C. Oleari and E. Re, *NLO single-top production matched with shower in POWHEG: s- and t-channel contributions*, *JHEP* **09** (2009) 111 [*Erratum ibid.* **1002** (2010) 011] [arXiv:0907.4076] [INSPIRE].

[55] J. Pumplin, D.R. Stump, J. Huston, H.L. Lai, P.M. Nadolsky and W.K. Tung, *New generation of parton distributions with uncertainties from global QCD analysis*, *JHEP* **07** (2002) 012 [hep-ph/0201195] [INSPIRE].

[56] R.D. Ball et al., *Impact of heavy quark masses on parton distributions and LHC phenomenology*, *Nucl. Phys.* **B 849** (2011) 296 [arXiv:1101.1300] [INSPIRE].

[57] CMS collaboration, *Study of the underlying event at forward rapidity in pp collisions at* $\sqrt{s} = 0.9$, 2.76 *and* 7 *TeV*, *JHEP* **04** (2013) 072 [arXiv:1302.2394] [INSPIRE].

[58] CMS collaboration, *Event generator tunes obtained from underlying event and multiparton scattering measurements*, *Eur. Phys. J.* **C 76** (2016) 155 [arXiv:1512.00815] [INSPIRE].

[59] GEANT4 collaboration, S. Agostinelli et al., *GEANT4: A simulation toolkit*, *Nucl. Instrum. Meth.* **A 506** (2003) 250 [INSPIRE].

[60] CMS collaboration, *Data parking and data scouting at the CMS experiment*, CMS-DP-2012-022 (2012).

[61] CMS collaboration, *Search for dark matter in proton-proton collisions at 8 TeV with missing transverse momentum and vector boson tagged jets*, *JHEP* **12** (2016) 083 [arXiv:1607.05764] [INSPIRE].

[62] CMS collaboration, *Performance of the CMS missing transverse momentum reconstruction in pp data at* $\sqrt{s} = 8$ *TeV*, 2015 *JINST* **10** P02006 [arXiv:1411.0511] [INSPIRE].

[63] CMS collaboration, *Measurement of the* $pp \to ZZ$ *production cross section and constraints on anomalous triple gauge couplings in four-lepton final states at* $\sqrt{s} = 8$ *TeV*, *Phys. Lett.* **B 740** (2015) 250 [arXiv:1406.0113] [INSPIRE].

[64] CMS collaboration, *Measurement of the* W^+W^- *cross section in pp collisions at* $\sqrt{s} = 8$ *TeV and limits on anomalous gauge couplings*, *Eur. Phys. J.* **C 76** (2016) 401 [arXiv:1507.03268] [INSPIRE].

[65] CMS collaboration, *Measurement of* W^+W^- *and ZZ production cross sections in pp collisions at* $\sqrt{s} = 8$ *TeV*, *Phys. Lett.* **B 721** (2013) 190 [arXiv:1301.4698] [INSPIRE].

[66] CMS collaboration, *Measurement of the ZZ production cross section and* $Z \to \ell^+\ell^-\ell'^+\ell'^-$ *branching fraction in pp collisions at* $\sqrt{s} = 13$ *TeV*, *Phys. Lett.* **B 763** (2016) 280 [arXiv:1607.08834] [INSPIRE].

[67] CMS collaboration, *Measurement of the WZ production cross section in pp collisions at* $\sqrt{s} = 13$ *TeV*, *Phys. Lett.* **B 766** (2017) 268 [arXiv:1607.06943] [INSPIRE].

[68] CMS collaboration, *Measurements of the* $t\bar{t}$ *production cross section in lepton+jets final states in pp collisions at 8 TeV and ratio of 8 to 7 TeV cross sections*, *Eur. Phys. J.* **C 77** (2017) 15 [arXiv:1602.09024] [INSPIRE].

[69] CMS collaboration, *Measurement of the t-channel single-top-quark production cross section and of the* $|V_{tb}|$ *CKM matrix element in pp collisions at* $\sqrt{s} = 8$ *TeV*, *JHEP* **06** (2014) 090 [arXiv:1403.7366] [INSPIRE].

[70] CMS collaboration, *Measurement of the top quark pair production cross section in proton-proton collisions at* $\sqrt{s} = 13$ *TeV*, *Phys. Rev. Lett.* **116** (2016) 052002 [arXiv:1510.05302] [INSPIRE].

[71] K. Arnold et al., *VBFNLO: A parton level Monte Carlo for processes with electroweak bosons — Manual for Version 2.5.0*, arXiv:1107.4038 [INSPIRE].

[72] J. Baglio et al., *Release note — VBFNLO 2.7.0*, arXiv:1404.3940 [INSPIRE].

[73] J.M. Campbell, R.K. Ellis and C. Williams, *Vector boson pair production at the LHC*, *JHEP* **07** (2011) 018 [arXiv:1105.0020] [INSPIRE].

[74] J. Butterworth et al., *PDF4LHC recommendations for LHC Run II*, *J. Phys.* **G 43** (2016) 023001 [arXiv:1510.03865] [INSPIRE].

[75] J. Thaler and K. Van Tilburg, *Identifying boosted objects with N-subjettiness*, *JHEP* **03** (2011) 015 [arXiv:1011.2268] [INSPIRE].

[76] J. Thaler and K. Van Tilburg, *Maximizing boosted top identification by minimizing N-subjettiness*, *JHEP* **02** (2012) 093 [arXiv:1108.2701] [INSPIRE].

[77] S.D. Ellis, C.K. Vermilion and J.R. Walsh, *Recombination algorithms and jet substructure: Pruning as a tool for heavy particle searches*, *Phys. Rev.* **D 81** (2010) 094023 [arXiv:0912.0033] [INSPIRE].

[78] S. Ask, M.A. Parker, T. Sandoval, M.E. Shea and W.J. Stirling, *Using gamma+jets production to calibrate the standard model Z($\to \nu\nu$)+jets background to new physics processes at the LHC*, *JHEP* **10** (2011) 058 [arXiv:1107.2803] [INSPIRE].

[79] J.H. Kuhn, A. Kulesza, S. Pozzorini and M. Schulze, *Electroweak corrections to hadronic photon production at large transverse momenta*, *JHEP* **03** (2006) 059 [hep-ph/0508253] [INSPIRE].

[80] S. Kallweit, J.M. Lindert, P. Maierhöfer, S. Pozzorini and M. Schönherr, *NLO electroweak automation and precise predictions for W+multijet production at the LHC*, *JHEP* **04** (2015) 012 [arXiv:1412.5157] [INSPIRE].

[81] S. Kallweit, J.M. Lindert, S. Pozzorini, M. Schönherr and P. Maierhöfer, *NLO QCD+EW automation and precise predictions for V+multijet production*, arXiv:1505.05704 [INSPIRE].

[82] S. Kallweit, J.M. Lindert, P. Maierhofer, S. Pozzorini and M. Schönherr, *NLO QCD+EW predictions for V+jets including off-shell vector-boson decays and multijet merging*, *JHEP* **04** (2016) 021 [arXiv:1511.08692] [INSPIRE].

[83] NNPDF collaboration, R.D. Ball et al., *Parton distributions for the LHC Run II*, *JHEP* **04** (2015) 040 [arXiv:1410.8849] [INSPIRE].

[84] T. Junk, *Confidence level computation for combining searches with small statistics*, *Nucl. Instrum. Meth.* **A 434** (1999) 435 [hep-ex/9902006] [INSPIRE].

[85] A.L. Read, *Presentation of search results: the CL_s technique*, *J. Phys.* **G 28** (2002) 2693 [INSPIRE].

[86] G. Cowan, K. Cranmer, E. Gross and O. Vitells, *Asymptotic formulae for likelihood-based tests of new physics*, *Eur. Phys. J.* **C 71** (2011) 1554 [*Erratum ibid.* **C 73** (2013) 2501] [arXiv:1007.1727] [INSPIRE].

[87] ATLAS, CMS and THE LHC HIGGS COMBINATION GROUP collaborations, *Procedure for the LHC Higgs boson search combination in Summer 2011*, ATL-PHYS-PUB-2011-11 (2011).

[88] CMS collaboration, *Search for the standard model Higgs boson produced in association with a W or a Z boson and decaying to bottom quarks*, *Phys. Rev.* **D 89** (2014) 012003 [arXiv:1310.3687] [INSPIRE].

[89] K. Hamilton, P. Nason and G. Zanderighi, *MINLO: multi-scale improved NLO*, *JHEP* **10** (2012) 155 [arXiv:1206.3572] [INSPIRE].

[90] S. Frixione and B.R. Webber, *Matching NLO QCD computations and parton shower simulations*, *JHEP* **06** (2002) 029 [hep-ph/0204244] [INSPIRE].

[91] M. Bahr et al., *HERWIG++ physics and manual*, *Eur. Phys. J.* **C 58** (2008) 639 [arXiv:0803.0883] [INSPIRE].

[92] S. Catani, D. de Florian, M. Grazzini and P. Nason, *Soft gluon resummation for Higgs boson production at hadron colliders*, *JHEP* **07** (2003) 028 [hep-ph/0306211] [INSPIRE].

[93] R.D. Young and A.W. Thomas, *Octet baryon masses and sigma terms from an* SU(3) *chiral extrapolation*, *Phys. Rev.* **D 81** (2010) 014503 [arXiv:0901.3310] [INSPIRE].

[94] MILC collaboration, D. Toussaint and W. Freeman, *The strange quark condensate in the nucleon in 2+1 flavor QCD*, *Phys. Rev. Lett.* **103** (2009) 122002 [arXiv:0905.2432] [INSPIRE].

[95] LUX collaboration, D.S. Akerib et al., *Results from a search for dark matter in the complete LUX exposure*, *Phys. Rev. Lett.* **118** (2017) 021303 [arXiv:1608.07648] [INSPIRE].

[96] PandaX-II collaboration, A. Tan et al., *Dark matter results from first 98.7 Days of data from the PandaX-II experiment*, *Phys. Rev. Lett.* **117** (2016) 121303 [arXiv:1607.07400] [INSPIRE].

[97] SuperCDMS collaboration, R. Agnese et al., *New results from the search for low-mass weakly interacting massive particles with the CDMS low ionization threshold experiment*, *Phys. Rev. Lett.* **116** (2016) 071301 [arXiv:1509.02448] [INSPIRE].

The CMS collaboration

Yerevan Physics Institute, Yerevan, Armenia

V. Khachatryan, A.M. Sirunyan, A. Tumasyan

Institut für Hochenergiephysik, Wien, Austria

W. Adam, E. Asilar, T. Bergauer, J. Brandstetter, E. Brondolin, M. Dragicevic, J. Erö, M. Flechl, M. Friedl, R. Frühwirth[1], V.M. Ghete, C. Hartl, N. Hörmann, J. Hrubec, M. Jeitler[1], A. König, I. Krätschmer, D. Liko, T. Matsushita, I. Mikulec, D. Rabady, N. Rad, B. Rahbaran, H. Rohringer, J. Schieck[1], J. Strauss, W. Waltenberger, C.-E. Wulz[1]

Institute for Nuclear Problems, Minsk, Belarus

O. Dvornikov, V. Makarenko, V. Zykunov

National Centre for Particle and High Energy Physics, Minsk, Belarus

V. Mossolov, N. Shumeiko, J. Suarez Gonzalez

Universiteit Antwerpen, Antwerpen, Belgium

S. Alderweireldt, E.A. De Wolf, X. Janssen, J. Lauwers, M. Van De Klundert, H. Van Haevermaet, P. Van Mechelen, N. Van Remortel, A. Van Spilbeeck

Vrije Universiteit Brussel, Brussel, Belgium

S. Abu Zeid, F. Blekman, J. D'Hondt, N. Daci, I. De Bruyn, K. Deroover, S. Lowette, S. Moortgat, L. Moreels, A. Olbrechts, Q. Python, S. Tavernier, W. Van Doninck, P. Van Mulders, I. Van Parijs

Université Libre de Bruxelles, Bruxelles, Belgium

H. Brun, B. Clerbaux, G. De Lentdecker, H. Delannoy, G. Fasanella, L. Favart, R. Goldouzian, A. Grebenyuk, G. Karapostoli, T. Lenzi, A. Léonard, J. Luetic, T. Maerschalk, A. Marinov, A. Randle-conde, T. Seva, C. Vander Velde, P. Vanlaer, R. Yonamine, F. Zenoni, F. Zhang[2]

Ghent University, Ghent, Belgium

A. Cimmino, T. Cornelis, D. Dobur, A. Fagot, G. Garcia, M. Gul, I. Khvastunov, D. Poyraz, S. Salva, R. Schöfbeck, A. Sharma, M. Tytgat, W. Van Driessche, E. Yazgan, N. Zaganidis

Université Catholique de Louvain, Louvain-la-Neuve, Belgium

H. Bakhshiansohi, C. Beluffi[3], O. Bondu, S. Brochet, G. Bruno, A. Caudron, S. De Visscher, C. Delaere, M. Delcourt, B. Francois, A. Giammanco, A. Jafari, P. Jez, M. Komm, V. Lemaitre, A. Magitteri, A. Mertens, M. Musich, C. Nuttens, K. Piotrzkowski, L. Quertenmont, M. Selvaggi, M. Vidal Marono, S. Wertz

Université de Mons, Mons, Belgium

N. Beliy

Centro Brasileiro de Pesquisas Fisicas, Rio de Janeiro, Brazil

W.L. Aldá Júnior, F.L. Alves, G.A. Alves, L. Brito, C. Hensel, A. Moraes, M.E. Pol, P. Rebello Teles

Universidade do Estado do Rio de Janeiro, Rio de Janeiro, Brazil

E. Belchior Batista Das Chagas, W. Carvalho, J. Chinellato[4], A. Custódio, E.M. Da Costa, G.G. Da Silveira[5], D. De Jesus Damiao, C. De Oliveira Martins, S. Fonseca De Souza, L.M. Huertas Guativa, H. Malbouisson, D. Matos Figueiredo, C. Mora Herrera, L. Mundim, H. Nogima, W.L. Prado Da Silva, A. Santoro, A. Sznajder, E.J. Tonelli Manganote[4], A. Vilela Pereira

Universidade Estadual Paulista[a], Universidade Federal do ABC[b], São Paulo, Brazil

S. Ahuja[a], C.A. Bernardes[b], S. Dogra[a], T.R. Fernandez Perez Tomei[a], E.M. Gregores[b], P.G. Mercadante[b], C.S. Moon[a], S.F. Novaes[a], Sandra S. Padula[a], D. Romero Abad[b], J.C. Ruiz Vargas

Institute for Nuclear Research and Nuclear Energy, Sofia, Bulgaria

A. Aleksandrov, R. Hadjiiska, P. Iaydjiev, M. Rodozov, S. Stoykova, G. Sultanov, M. Vutova

University of Sofia, Sofia, Bulgaria

A. Dimitrov, I. Glushkov, L. Litov, B. Pavlov, P. Petkov

Beihang University, Beijing, China

W. Fang[6]

Institute of High Energy Physics, Beijing, China

M. Ahmad, J.G. Bian, G.M. Chen, H.S. Chen, M. Chen, Y. Chen[7], T. Cheng, C.H. Jiang, D. Leggat, Z. Liu, F. Romeo, S.M. Shaheen, A. Spiezia, J. Tao, C. Wang, Z. Wang, H. Zhang, J. Zhao

State Key Laboratory of Nuclear Physics and Technology, Peking University, Beijing, China

Y. Ban, G. Chen, Q. Li, S. Liu, Y. Mao, S.J. Qian, D. Wang, Z. Xu

Universidad de Los Andes, Bogota, Colombia

C. Avila, A. Cabrera, L.F. Chaparro Sierra, C. Florez, J.P. Gomez, C.F. González Hernández, J.D. Ruiz Alvarez, J.C. Sanabria

University of Split, Faculty of Electrical Engineering, Mechanical Engineering and Naval Architecture, Split, Croatia

N. Godinovic, D. Lelas, I. Puljak, P.M. Ribeiro Cipriano, T. Sculac

University of Split, Faculty of Science, Split, Croatia

Z. Antunovic, M. Kovac

Institute Rudjer Boskovic, Zagreb, Croatia

V. Brigljevic, D. Ferencek, K. Kadija, S. Micanovic, L. Sudic, T. Susa

University of Cyprus, Nicosia, Cyprus

A. Attikis, G. Mavromanolakis, J. Mousa, C. Nicolaou, F. Ptochos, P.A. Razis, H. Rykaczewski, D. Tsiakkouri

Charles University, Prague, Czech Republic

M. Finger[8], M. Finger Jr.[8]

Universidad San Francisco de Quito, Quito, Ecuador

E. Carrera Jarrin

Academy of Scientific Research and Technology of the Arab Republic of Egypt, Egyptian Network of High Energy Physics, Cairo, Egypt

Y. Assran[9,10], T. Elkafrawy[11], A. Mahrous[12]

National Institute of Chemical Physics and Biophysics, Tallinn, Estonia

B. Calpas, M. Kadastik, M. Murumaa, L. Perrini, M. Raidal, A. Tiko, C. Veelken

Department of Physics, University of Helsinki, Helsinki, Finland

P. Eerola, J. Pekkanen, M. Voutilainen

Helsinki Institute of Physics, Helsinki, Finland

J. Härkönen, T. Järvinen, V. Karimäki, R. Kinnunen, T. Lampén, K. Lassila-Perini, S. Lehti, T. Lindén, P. Luukka, J. Tuominiemi, E. Tuovinen, L. Wendland

Lappeenranta University of Technology, Lappeenranta, Finland

J. Talvitie, T. Tuuva

IRFU, CEA, Université Paris-Saclay, Gif-sur-Yvette, France

M. Besancon, F. Couderc, M. Dejardin, D. Denegri, B. Fabbro, J.L. Faure, C. Favaro, F. Ferri, S. Ganjour, S. Ghosh, A. Givernaud, P. Gras, G. Hamel de Monchenault, P. Jarry, I. Kucher, E. Locci, M. Machet, J. Malcles, J. Rander, A. Rosowsky, M. Titov, A. Zghiche

Laboratoire Leprince-Ringuet, Ecole Polytechnique, IN2P3-CNRS, Palaiseau, France

A. Abdulsalam, I. Antropov, S. Baffioni, F. Beaudette, P. Busson, L. Cadamuro, E. Chapon, C. Charlot, O. Davignon, R. Granier de Cassagnac, M. Jo, S. Lisniak, P. Miné, M. Nguyen, C. Ochando, G. Ortona, P. Paganini, P. Pigard, S. Regnard, R. Salerno, Y. Sirois, T. Strebler, Y. Yilmaz, A. Zabi

Institut Pluridisciplinaire Hubert Curien, Université de Strasbourg, Université de Haute Alsace Mulhouse, CNRS/IN2P3, Strasbourg, France

J.-L. Agram[13], J. Andrea, A. Aubin, D. Bloch, J.-M. Brom, M. Buttignol, E.C. Chabert, N. Chanon, C. Collard, E. Conte[13], X. Coubez, J.-C. Fontaine[13], D. Gelé, U. Goerlach, A.-C. Le Bihan, K. Skovpen, P. Van Hove

Centre de Calcul de l'Institut National de Physique Nucleaire et de Physique des Particules, CNRS/IN2P3, Villeurbanne, France

S. Gadrat

Université de Lyon, Université Claude Bernard Lyon 1, CNRS-IN2P3, Institut de Physique Nucléaire de Lyon, Villeurbanne, France

S. Beauceron, C. Bernet, G. Boudoul, E. Bouvier, C.A. Carrillo Montoya, R. Chierici, D. Contardo, B. Courbon, P. Depasse, H. El Mamouni, J. Fan, J. Fay, S. Gascon,

M. Gouzevitch, G. Grenier, B. Ille, F. Lagarde, I.B. Laktineh, M. Lethuillier, L. Mirabito,
A.L. Pequegnot, S. Perries, A. Popov[14], D. Sabes, V. Sordini, M. Vander Donckt, P. Verdier,
S. Viret

Georgian Technical University, Tbilisi, Georgia

T. Toriashvili[15]

Tbilisi State University, Tbilisi, Georgia

Z. Tsamalaidze[8]

RWTH Aachen University, I. Physikalisches Institut, Aachen, Germany

C. Autermann, S. Beranek, L. Feld, A. Heister, M.K. Kiesel, K. Klein, M. Lipinski,
A. Ostapchuk, M. Preuten, F. Raupach, S. Schael, C. Schomakers, J. Schulz, T. Verlage,
H. Weber

RWTH Aachen University, III. Physikalisches Institut A, Aachen, Germany

A. Albert, M. Brodski, E. Dietz-Laursonn, D. Duchardt, M. Endres, M. Erdmann,
S. Erdweg, T. Esch, R. Fischer, A. Güth, M. Hamer, T. Hebbeker, C. Heidemann,
K. Hoepfner, S. Knutzen, M. Merschmeyer, A. Meyer, P. Millet, S. Mukherjee,
M. Olschewski, K. Padeken, T. Pook, M. Radziej, H. Reithler, M. Rieger, F. Scheuch,
L. Sonnenschein, D. Teyssier, S. Thüer

RWTH Aachen University, III. Physikalisches Institut B, Aachen, Germany

V. Cherepanov, G. Flügge, F. Hoehle, B. Kargoll, T. Kress, A. Künsken, J. Lingemann,
T. Müller, A. Nehrkorn, A. Nowack, I.M. Nugent, C. Pistone, O. Pooth, A. Stahl[16]

Deutsches Elektronen-Synchrotron, Hamburg, Germany

M. Aldaya Martin, T. Arndt, C. Asawatangtrakuldee, K. Beernaert, O. Behnke,
U. Behrens, A.A. Bin Anuar, K. Borras[17], A. Campbell, P. Connor, C. Contreras-Campana,
F. Costanza, C. Diez Pardos, G. Dolinska, G. Eckerlin, D. Eckstein, T. Eichhorn, E. Eren,
E. Gallo[18], J. Garay Garcia, A. Geiser, A. Gizhko, J.M. Grados Luyando, P. Gun-
nellini, A. Harb, J. Hauk, M. Hempel[19], H. Jung, A. Kalogeropoulos, O. Karacheban[19],
M. Kasemann, J. Keaveney, C. Kleinwort, I. Korol, D. Krücker, W. Lange, A. Lelek,
J. Leonard, K. Lipka, A. Lobanov, W. Lohmann[19], R. Mankel, I.-A. Melzer-Pellmann,
A.B. Meyer, G. Mittag, J. Mnich, A. Mussgiller, E. Ntomari, D. Pitzl, R. Placakyte,
A. Raspereza, B. Roland, M.Ö. Sahin, P. Saxena, T. Schoerner-Sadenius, C. Seitz,
S. Spannagel, N. Stefaniuk, G.P. Van Onsem, R. Walsh, C. Wissing

University of Hamburg, Hamburg, Germany

V. Blobel, M. Centis Vignali, A.R. Draeger, T. Dreyer, E. Garutti, D. Gonzalez, J. Haller,
M. Hoffmann, A. Junkes, R. Klanner, R. Kogler, N. Kovalchuk, T. Lapsien, T. Lenz,
I. Marchesini, D. Marconi, M. Meyer, M. Niedziela, D. Nowatschin, F. Pantaleo[16],
T. Peiffer, A. Perieanu, J. Poehlsen, C. Sander, C. Scharf, P. Schleper, A. Schmidt,
S. Schumann, J. Schwandt, H. Stadie, G. Steinbrück, F.M. Stober, M. Stöver, H. Tholen,
D. Troendle, E. Usai, L. Vanelderen, A. Vanhoefer, B. Vormwald

Institut für Experimentelle Kernphysik, Karlsruhe, Germany

M. Akbiyik, C. Barth, S. Baur, C. Baus, J. Berger, E. Butz, R. Caspart, T. Chwalek, F. Colombo, W. De Boer, A. Dierlamm, S. Fink, B. Freund, R. Friese, M. Giffels, A. Gilbert, P. Goldenzweig, D. Haitz, F. Hartmann[16], S.M. Heindl, U. Husemann, I. Katkov[14], S. Kudella, P. Lobelle Pardo, H. Mildner, M.U. Mozer, Th. Müller, M. Plagge, G. Quast, K. Rabbertz, S. Röcker, F. Roscher, M. Schröder, I. Shvetsov, G. Sieber, H.J. Simonis, R. Ulrich, J. Wagner-Kuhr, S. Wayand, M. Weber, T. Weiler, S. Williamson, C. Wöhrmann, R. Wolf

Institute of Nuclear and Particle Physics (INPP), NCSR Demokritos, Aghia Paraskevi, Greece

G. Anagnostou, G. Daskalakis, T. Geralis, V.A. Giakoumopoulou, A. Kyriakis, D. Loukas, I. Topsis-Giotis

National and Kapodistrian University of Athens, Athens, Greece

S. Kesisoglou, A. Panagiotou, N. Saoulidou, E. Tziaferi

University of Ioánnina, Ioánnina, Greece

I. Evangelou, G. Flouris, C. Foudas, P. Kokkas, N. Loukas, N. Manthos, I. Papadopoulos, E. Paradas

MTA-ELTE Lendület CMS Particle and Nuclear Physics Group, Eötvös Loránd University, Budapest, Hungary

N. Filipovic

Wigner Research Centre for Physics, Budapest, Hungary

G. Bencze, C. Hajdu, P. Hidas, D. Horvath[20], F. Sikler, V. Veszpremi, G. Vesztergombi[21], A.J. Zsigmond

Institute of Nuclear Research ATOMKI, Debrecen, Hungary

N. Beni, S. Czellar, J. Karancsi[22], A. Makovec, J. Molnar, Z. Szillasi

University of Debrecen, Debrecen, Hungary

M. Bartók[21], P. Raics, Z.L. Trocsanyi, B. Ujvari

National Institute of Science Education and Research, Bhubaneswar, India

S. Bahinipati, S. Choudhury[23], P. Mal, K. Mandal, A. Nayak[24], D.K. Sahoo, N. Sahoo, S.K. Swain

Panjab University, Chandigarh, India

S. Bansal, S.B. Beri, V. Bhatnagar, R. Chawla, U.Bhawandeep, A.K. Kalsi, A. Kaur, M. Kaur, R. Kumar, P. Kumari, A. Mehta, M. Mittal, J.B. Singh, G. Walia

University of Delhi, Delhi, India

Ashok Kumar, A. Bhardwaj, B.C. Choudhary, R.B. Garg, S. Keshri, S. Malhotra, M. Naimuddin, N. Nishu, K. Ranjan, R. Sharma, V. Sharma

Saha Institute of Nuclear Physics, Kolkata, India

R. Bhattacharya, S. Bhattacharya, K. Chatterjee, S. Dey, S. Dutt, S. Dutta, S. Ghosh, N. Majumdar, A. Modak, K. Mondal, S. Mukhopadhyay, S. Nandan, A. Purohit, A. Roy, D. Roy, S. Roy Chowdhury, S. Sarkar, M. Sharan, S. Thakur

Indian Institute of Technology Madras, Madras, India

P.K. Behera

Bhabha Atomic Research Centre, Mumbai, India

R. Chudasama, D. Dutta, V. Jha, V. Kumar, A.K. Mohanty[16], P.K. Netrakanti, L.M. Pant, P. Shukla, A. Topkar

Tata Institute of Fundamental Research-A, Mumbai, India

T. Aziz, S. Dugad, G. Kole, B. Mahakud, S. Mitra, G.B. Mohanty, B. Parida, N. Sur, B. Sutar

Tata Institute of Fundamental Research-B, Mumbai, India

S. Banerjee, S. Bhowmik[25], R.K. Dewanjee, S. Ganguly, M. Guchait, Sa. Jain, S. Kumar, M. Maity[25], G. Majumder, K. Mazumdar, T. Sarkar[25], N. Wickramage[26]

Indian Institute of Science Education and Research (IISER), Pune, India

S. Chauhan, S. Dube, V. Hegde, A. Kapoor, K. Kothekar, A. Rane, S. Sharma

Institute for Research in Fundamental Sciences (IPM), Tehran, Iran

H. Behnamian, S. Chenarani[27], E. Eskandari Tadavani, S.M. Etesami[27], A. Fahim[28], M. Khakzad, M. Mohammadi Najafabadi, M. Naseri, S. Paktinat Mehdiabadi[29], F. Rezaei Hosseinabadi, B. Safarzadeh[30], M. Zeinali

University College Dublin, Dublin, Ireland

M. Felcini, M. Grunewald

INFN Sezione di Bari ^{a}, Università di Bari ^{b}, Politecnico di Bari ^{c}, Bari, Italy

M. Abbrescia^{a,b}, C. Calabria^{a,b}, C. Caputo^{a,b}, A. Colaleo^a, D. Creanza^{a,c}, L. Cristella^{a,b}, N. De Filippis^{a,c}, M. De Palma^{a,b}, L. Fiore^a, G. Iaselli^{a,c}, G. Maggi^{a,c}, M. Maggi^a, G. Miniello^{a,b}, S. My^{a,b}, S. Nuzzo^{a,b}, A. Pompili^{a,b}, G. Pugliese^{a,c}, R. Radogna^{a,b}, A. Ranieri^a, G. Selvaggi^{a,b}, L. Silvestris^{a,16}, R. Venditti^{a,b}, P. Verwilligen^a

INFN Sezione di Bologna ^{a}, Università di Bologna ^{b}, Bologna, Italy

G. Abbiendi^a, C. Battilana, D. Bonacorsi^{a,b}, S. Braibant-Giacomelli^{a,b}, L. Brigliadori^{a,b}, R. Campanini^{a,b}, P. Capiluppi^{a,b}, A. Castro^{a,b}, F.R. Cavallo^a, S.S. Chhibra^{a,b}, G. Codispoti^{a,b}, M. Cuffiani^{a,b}, G.M. Dallavalle^a, F. Fabbri^a, A. Fanfani^{a,b}, D. Fasanella^{a,b}, P. Giacomelli^a, C. Grandi^a, L. Guiducci^{a,b}, S. Marcellini^a, G. Masetti^a, A. Montanari^a, F.L. Navarria^{a,b}, A. Perrotta^a, A.M. Rossi^{a,b}, T. Rovelli^{a,b}, G.P. Siroli^{a,b}, N. Tosi^{a,b,16}

INFN Sezione di Catania ^{a}, Università di Catania ^{b}, Catania, Italy

S. Albergo^{a,b}, M. Chiorboli^{a,b}, S. Costa^{a,b}, A. Di Mattia^a, F. Giordano^{a,b}, R. Potenza^{a,b}, A. Tricomi^{a,b}, C. Tuve^{a,b}

INFN Sezione di Firenze ^{a}, Università di Firenze ^{b}, Firenze, Italy

G. Barbagli^a, V. Ciulli^{a,b}, C. Civinini^a, R. D'Alessandro^{a,b}, E. Focardi^{a,b}, V. Gori^{a,b}, P. Lenzi^{a,b}, M. Meschini^a, S. Paoletti^a, G. Sguazzoni^a, L. Viliani^{a,b,16}

INFN Laboratori Nazionali di Frascati, Frascati, Italy

L. Benussi, S. Bianco, F. Fabbri, D. Piccolo, F. Primavera^{16}

INFN Sezione di Genova ^{a}, Università di Genova ^{b}, Genova, Italy

V. Calvelli^{a,b}, F. Ferro^a, M. Lo Vetere^{a,b}, M.R. Monge^{a,b}, E. Robutti^a, S. Tosi^{a,b}

INFN Sezione di Milano-Bicocca ^{a}, Università di Milano-Bicocca ^{b}, Milano, Italy

L. Brianza^{16}, M.E. Dinardo^{a,b}, S. Fiorendi^{a,b}, S. Gennai^a, A. Ghezzi^{a,b}, P. Govoni^{a,b}, M. Malberti, S. Malvezzi^a, R.A. Manzoni^{a,b,16}, D. Menasce^a, L. Moroni^a, M. Paganoni^{a,b}, D. Pedrini^a, S. Pigazzini, S. Ragazzi^{a,b}, T. Tabarelli de Fatis^{a,b}

INFN Sezione di Napoli ^{a}, Università di Napoli 'Federico II' ^{b}, Napoli, Italy, Università della Basilicata ^{c}, Potenza, Italy, Università G. Marconi ^{d}, Roma, Italy

S. Buontempo^a, N. Cavallo^{a,c}, G. De Nardo, S. Di Guida^{a,d,16}, M. Esposito^{a,b}, F. Fabozzi^{a,c}, F. Fienga^{a,b}, A.O.M. Iorio^{a,b}, G. Lanza^a, L. Lista^a, S. Meola^{a,d,16}, P. Paolucci^{a,16}, C. Sciacca^{a,b}, F. Thyssen

INFN Sezione di Padova ^{a}, Università di Padova ^{b}, Padova, Italy, Università di Trento ^{c}, Trento, Italy

P. Azzi^{a,16}, N. Bacchetta^a, L. Benato^{a,b}, D. Bisello^{a,b}, A. Boletti^{a,b}, R. Carlin^{a,b}, A. Carvalho Antunes De Oliveira^{a,b}, P. Checchia^a, M. Dall'Osso^{a,b}, P. De Castro Manzano^a, T. Dorigo^a, U. Dosselli^a, F. Gasparini^{a,b}, U. Gasparini^{a,b}, A. Gozzelino^a, S. Lacaprara^a, M. Margoni^{a,b}, A.T. Meneguzzo^{a,b}, J. Pazzini^{a,b}, N. Pozzobon^{a,b}, P. Ronchese^{a,b}, F. Simonetto^{a,b}, E. Torassa^a, M. Zanetti, P. Zotto^{a,b}, G. Zumerle^{a,b}

INFN Sezione di Pavia ^{a}, Università di Pavia ^{b}, Pavia, Italy

A. Braghieri^a, A. Magnani^{a,b}, P. Montagna^{a,b}, S.P. Ratti^{a,b}, V. Re^a, C. Riccardi^{a,b}, P. Salvini^a, I. Vai^{a,b}, P. Vitulo^{a,b}

INFN Sezione di Perugia ^{a}, Università di Perugia ^{b}, Perugia, Italy

L. Alunni Solestizi^{a,b}, G.M. Bilei^a, D. Ciangottini^{a,b}, L. Fanò^{a,b}, P. Lariccia^{a,b}, R. Leonardi^{a,b}, G. Mantovani^{a,b}, M. Menichelli^a, A. Saha^a, A. Santocchia^{a,b}

INFN Sezione di Pisa ^{a}, Università di Pisa ^{b}, Scuola Normale Superiore di Pisa ^{c}, Pisa, Italy

K. Androsov^{a,31}, P. Azzurri^{a,16}, G. Bagliesi^a, J. Bernardini^a, T. Boccali^a, R. Castaldi^a, M.A. Ciocci^{a,31}, R. Dell'Orso^a, S. Donato^{a,c}, G. Fedi, A. Giassi^a, M.T. Grippo^{a,31}, F. Ligabue^{a,c}, T. Lomtadze^a, L. Martini^{a,b}, A. Messineo^{a,b}, F. Palla^a, A. Rizzi^{a,b}, A. Savoy-Navarro^{a,32}, P. Spagnolo^a, R. Tenchini^a, G. Tonelli^{a,b}, A. Venturi^a, P.G. Verdini^a

INFN Sezione di Roma ^{a}, Università di Roma ^{b}, Roma, Italy

L. Barone^{a,b}, F. Cavallari^a, M. Cipriani^{a,b}, D. Del Re^{a,b,16}, M. Diemoz^a, S. Gelli^{a,b}, E. Longo^{a,b}, F. Margaroli^{a,b}, B. Marzocchi^{a,b}, P. Meridiani^a, G. Organtini^{a,b}, R. Paramatti^a, F. Preiato^{a,b}, S. Rahatlou^{a,b}, C. Rovelli^a, F. Santanastasio^{a,b}

INFN Sezione di Torino ^{a}, Università di Torino ^{b}, Torino, Italy, Università del Piemonte Orientale ^{c}, Novara, Italy

N. Amapane^{a,b}, R. Arcidiacono^{a,c,16}, S. Argiro^{a,b}, M. Arneodo^{a,c}, N. Bartosik^a, R. Bellan^{a,b}, C. Biino^a, N. Cartiglia^a, F. Cenna^{a,b}, M. Costa^{a,b}, R. Covarelli^{a,b}, A. Degano^{a,b}, N. Demaria^a, L. Finco^{a,b}, B. Kiani^{a,b}, C. Mariotti^a, S. Maselli^a, E. Migliore^{a,b}, V. Monaco^{a,b}, E. Monteil^{a,b}, M.M. Obertino^{a,b}, L. Pacher^{a,b}, N. Pastrone^a, M. Pelliccioni^a, G.L. Pinna Angioni^{a,b}, F. Ravera^{a,b}, A. Romero^{a,b}, M. Ruspa^{a,c}, R. Sacchi^{a,b}, K. Shchelina^{a,b}, V. Sola^a, A. Solano^{a,b}, A. Staiano^a, P. Traczyk^{a,b}

INFN Sezione di Trieste ^{a}, Università di Trieste ^{b}, Trieste, Italy

S. Belforte^a, M. Casarsa^a, F. Cossutti^a, G. Della Ricca^{a,b}, A. Zanetti^a

Kyungpook National University, Daegu, Korea

D.H. Kim, G.N. Kim, M.S. Kim, S. Lee, S.W. Lee, Y.D. Oh, S. Sekmen, D.C. Son, Y.C. Yang

Chonbuk National University, Jeonju, Korea

A. Lee

Chonnam National University, Institute for Universe and Elementary Particles, Kwangju, Korea

H. Kim

Hanyang University, Seoul, Korea

J.A. Brochero Cifuentes, T.J. Kim

Korea University, Seoul, Korea

S. Cho, S. Choi, Y. Go, D. Gyun, S. Ha, B. Hong, Y. Jo, Y. Kim, B. Lee, K. Lee, K.S. Lee, S. Lee, J. Lim, S.K. Park, Y. Roh

Seoul National University, Seoul, Korea

J. Almond, J. Kim, H. Lee, S.B. Oh, B.C. Radburn-Smith, S.h. Seo, U.K. Yang, H.D. Yoo, G.B. Yu

University of Seoul, Seoul, Korea

M. Choi, H. Kim, J.H. Kim, J.S.H. Lee, I.C. Park, G. Ryu, M.S. Ryu

Sungkyunkwan University, Suwon, Korea

Y. Choi, J. Goh, C. Hwang, J. Lee, I. Yu

Vilnius University, Vilnius, Lithuania

V. Dudenas, A. Juodagalvis, J. Vaitkus

National Centre for Particle Physics, Universiti Malaya, Kuala Lumpur, Malaysia

I. Ahmed, Z.A. Ibrahim, J.R. Komaragiri, M.A.B. Md Ali[33], F. Mohamad Idris[34], W.A.T. Wan Abdullah, M.N. Yusli, Z. Zolkapli

Centro de Investigacion y de Estudios Avanzados del IPN, Mexico City, Mexico

H. Castilla-Valdez, E. De La Cruz-Burelo, I. Heredia-De La Cruz[35], A. Hernandez-Almada, R. Lopez-Fernandez, R. Magaña Villalba, J. Mejia Guisao, A. Sanchez-Hernandez

Universidad Iberoamericana, Mexico City, Mexico

S. Carrillo Moreno, C. Oropeza Barrera, F. Vazquez Valencia

Benemerita Universidad Autonoma de Puebla, Puebla, Mexico

S. Carpinteyro, I. Pedraza, H.A. Salazar Ibarguen, C. Uribe Estrada

Universidad Autónoma de San Luis Potosí, San Luis Potosí, Mexico

A. Morelos Pineda

University of Auckland, Auckland, New Zealand

D. Krofcheck

University of Canterbury, Christchurch, New Zealand

P.H. Butler

National Centre for Physics, Quaid-I-Azam University, Islamabad, Pakistan

A. Ahmad, M. Ahmad, Q. Hassan, H.R. Hoorani, W.A. Khan, A. Saddique, M.A. Shah, M. Shoaib, M. Waqas

National Centre for Nuclear Research, Swierk, Poland

H. Bialkowska, M. Bluj, B. Boimska, T. Frueboes, M. Górski, M. Kazana, K. Nawrocki, K. Romanowska-Rybinska, M. Szleper, P. Zalewski

Institute of Experimental Physics, Faculty of Physics, University of Warsaw, Warsaw, Poland

K. Bunkowski, A. Byszuk[36], K. Doroba, A. Kalinowski, M. Konecki, J. Krolikowski, M. Misiura, M. Olszewski, M. Walczak

Laboratório de Instrumentação e Física Experimental de Partículas, Lisboa, Portugal

P. Bargassa, C. Beirão Da Cruz E Silva, A. Di Francesco, P. Faccioli, P.G. Ferreira Parracho, M. Gallinaro, J. Hollar, N. Leonardo, L. Lloret Iglesias, M.V. Nemallapudi, J. Rodrigues Antunes, J. Seixas, O. Toldaiev, D. Vadruccio, J. Varela, P. Vischia

Joint Institute for Nuclear Research, Dubna, Russia

P. Bunin, M. Gavrilenko, I. Golutvin, I. Gorbunov, A. Kamenev, V. Karjavin, A. Lanev, A. Malakhov, V. Matveev[37,38], V. Palichik, V. Perelygin, M. Savina, S. Shmatov, S. Shulha, N. Skatchkov, V. Smirnov, N. Voytishin, A. Zarubin

Petersburg Nuclear Physics Institute, Gatchina (St. Petersburg), Russia

L. Chtchipounov, V. Golovtsov, Y. Ivanov, V. Kim[39], E. Kuznetsova[40], V. Murzin, V. Oreshkin, V. Sulimov, A. Vorobyev

Institute for Nuclear Research, Moscow, Russia

Yu. Andreev, A. Dermenev, S. Gninenko, N. Golubev, A. Karneyeu, M. Kirsanov, N. Krasnikov, A. Pashenkov, D. Tlisov, A. Toropin

Institute for Theoretical and Experimental Physics, Moscow, Russia

V. Epshteyn, V. Gavrilov, N. Lychkovskaya, V. Popov, I. Pozdnyakov, G. Safronov, A. Spiridonov, M. Toms, E. Vlasov, A. Zhokin

Moscow Institute of Physics and Technology

A. Bylinkin[38]

National Research Nuclear University 'Moscow Engineering Physics Institute' (MEPhI), Moscow, Russia

R. Chistov[41], M. Danilov[41], V. Rusinov

P.N. Lebedev Physical Institute, Moscow, Russia

V. Andreev, M. Azarkin[38], I. Dremin[38], M. Kirakosyan, A. Leonidov[38], S.V. Rusakov, A. Terkulov

Skobeltsyn Institute of Nuclear Physics, Lomonosov Moscow State University, Moscow, Russia

A. Baskakov, A. Belyaev, E. Boos, V. Bunichev, M. Dubinin[42], L. Dudko, A. Gribushin, V. Klyukhin, O. Kodolova, I. Lokhtin, I. Miagkov, S. Obraztsov, M. Perfilov, S. Petrushanko, V. Savrin

Novosibirsk State University (NSU), Novosibirsk, Russia

V. Blinov[43], Y.Skovpen[43]

State Research Center of Russian Federation, Institute for High Energy Physics, Protvino, Russia

I. Azhgirey, I. Bayshev, S. Bitioukov, D. Elumakhov, V. Kachanov, A. Kalinin, D. Konstantinov, V. Krychkine, V. Petrov, R. Ryutin, A. Sobol, S. Troshin, N. Tyurin, A. Uzunian, A. Volkov

University of Belgrade, Faculty of Physics and Vinca Institute of Nuclear Sciences, Belgrade, Serbia

P. Adzic[44], P. Cirkovic, D. Devetak, M. Dordevic, J. Milosevic, V. Rekovic

Centro de Investigaciones Energéticas Medioambientales y Tecnológicas (CIEMAT), Madrid, Spain

J. Alcaraz Maestre, M. Barrio Luna, E. Calvo, M. Cerrada, M. Chamizo Llatas, N. Colino, B. De La Cruz, A. Delgado Peris, A. Escalante Del Valle, C. Fernandez Bedoya, J.P. Fernández Ramos, J. Flix, M.C. Fouz, P. Garcia-Abia,

O. Gonzalez Lopez, S. Goy Lopez, J.M. Hernandez, M.I. Josa, E. Navarro De Martino, A. Pérez-Calero Yzquierdo, J. Puerta Pelayo, A. Quintario Olmeda, I. Redondo, L. Romero, M.S. Soares

Universidad Autónoma de Madrid, Madrid, Spain

J.F. de Trocóniz, M. Missiroli, D. Moran

Universidad de Oviedo, Oviedo, Spain

J. Cuevas, J. Fernandez Menendez, I. Gonzalez Caballero, J.R. González Fernández, E. Palencia Cortezon, S. Sanchez Cruz, I. Suárez Andrés, J.M. Vizan Garcia

Instituto de Física de Cantabria (IFCA), CSIC-Universidad de Cantabria, Santander, Spain

I.J. Cabrillo, A. Calderon, J.R. Castiñeiras De Saa, E. Curras, M. Fernandez, J. Garcia-Ferrero, G. Gomez, A. Lopez Virto, J. Marco, C. Martinez Rivero, F. Matorras, J. Piedra Gomez, T. Rodrigo, A. Ruiz-Jimeno, L. Scodellaro, N. Trevisani, I. Vila, R. Vilar Cortabitarte

CERN, European Organization for Nuclear Research, Geneva, Switzerland

D. Abbaneo, E. Auffray, G. Auzinger, M. Bachtis, P. Baillon, A.H. Ball, D. Barney, P. Bloch, A. Bocci, A. Bonato, C. Botta, T. Camporesi, R. Castello, M. Cepeda, G. Cerminara, M. D'Alfonso, D. d'Enterria, A. Dabrowski, V. Daponte, A. David, M. De Gruttola, A. De Roeck, E. Di Marco[45], M. Dobson, B. Dorney, T. du Pree, D. Duggan, M. Dünser, N. Dupont, A. Elliott-Peisert, S. Fartoukh, G. Franzoni, J. Fulcher, W. Funk, D. Gigi, K. Gill, M. Girone, F. Glege, D. Gulhan, S. Gundacker, M. Guthoff, J. Hammer, P. Harris, J. Hegeman, V. Innocente, P. Janot, J. Kieseler, H. Kirschenmann, V. Knünz, A. Kornmayer[16], M.J. Kortelainen, K. Kousouris, M. Krammer[1], C. Lange, P. Lecoq, C. Lourenço, M.T. Lucchini, L. Malgeri, M. Mannelli, A. Martelli, F. Meijers, J.A. Merlin, S. Mersi, E. Meschi, F. Moortgat, S. Morovic, M. Mulders, H. Neugebauer, S. Orfanelli, L. Orsini, L. Pape, E. Perez, M. Peruzzi, A. Petrilli, G. Petrucciani, A. Pfeiffer, M. Pierini, A. Racz, T. Reis, G. Rolandi[46], M. Rovere, M. Ruan, H. Sakulin, J.B. Sauvan, C. Schäfer, C. Schwick, M. Seidel, A. Sharma, P. Silva, P. Sphicas[47], J. Steggemann, M. Stoye, Y. Takahashi, M. Tosi, D. Treille, A. Triossi, A. Tsirou, V. Veckalns[48], G.I. Veres[21], N. Wardle, A. Zagozdzinska[36], W.D. Zeuner

Paul Scherrer Institut, Villigen, Switzerland

W. Bertl, K. Deiters, W. Erdmann, R. Horisberger, Q. Ingram, H.C. Kaestli, D. Kotlinski, T. Rohe

Institute for Particle Physics, ETH Zurich, Zurich, Switzerland

F. Bachmair, L. Bäni, L. Bianchini, B. Casal, G. Dissertori, M. Dittmar, M. Donegà, C. Grab, C. Heidegger, D. Hits, J. Hoss, G. Kasieczka, P. Lecomte[†], W. Lustermann, B. Mangano, M. Marionneau, P. Martinez Ruiz del Arbol, M. Masciovecchio, M.T. Meinhard, D. Meister, F. Micheli, P. Musella, F. Nessi-Tedaldi, F. Pandolfi, J. Pata, F. Pauss, G. Perrin, L. Perrozzi, M. Quittnat, M. Rossini, M. Schönenberger, A. Starodumov[49], V.R. Tavolaro, K. Theofilatos, R. Wallny

Universität Zürich, Zurich, Switzerland

T.K. Aarrestad, C. Amsler[50], L. Caminada, M.F. Canelli, A. De Cosa, C. Galloni, A. Hinzmann, T. Hreus, B. Kilminster, J. Ngadiuba, D. Pinna, G. Rauco, P. Robmann, D. Salerno, Y. Yang, A. Zucchetta

National Central University, Chung-Li, Taiwan

V. Candelise, T.H. Doan, Sh. Jain, R. Khurana, M. Konyushikhin, C.M. Kuo, W. Lin, Y.J. Lu, A. Pozdnyakov, S.S. Yu

National Taiwan University (NTU), Taipei, Taiwan

Arun Kumar, P. Chang, Y.H. Chang, Y.W. Chang, Y. Chao, K.F. Chen, P.H. Chen, C. Dietz, F. Fiori, W.-S. Hou, Y. Hsiung, Y.F. Liu, R.-S. Lu, M. Miñano Moya, E. Paganis, A. Psallidas, J.f. Tsai, Y.M. Tzeng

Chulalongkorn University, Faculty of Science, Department of Physics, Bangkok, Thailand

B. Asavapibhop, G. Singh, N. Srimanobhas, N. Suwonjandee

Cukurova University, Adana, Turkey

A. Adiguzel, M.N. Bakirci[51], S. Damarseckin, Z.S. Demiroglu, C. Dozen, E. Eskut, S. Girgis, G. Gokbulut, Y. Guler, I. Hos, E.E. Kangal[52], O. Kara, U. Kiminsu, M. Oglakci, G. Onengut[53], K. Ozdemir[54], S. Ozturk[51], A. Polatoz, D. Sunar Cerci[55], S. Turkcapar, I.S. Zorbakir, C. Zorbilmez

Middle East Technical University, Physics Department, Ankara, Turkey

B. Bilin, S. Bilmis, B. Isildak[56], G. Karapinar[57], M. Yalvac, M. Zeyrek

Bogazici University, Istanbul, Turkey

E. Gülmez, M. Kaya[58], O. Kaya[59], E.A. Yetkin[60], T. Yetkin[61]

Istanbul Technical University, Istanbul, Turkey

A. Cakir, K. Cankocak, S. Sen[62]

Institute for Scintillation Materials of National Academy of Science of Ukraine, Kharkov, Ukraine

B. Grynyov

National Scientific Center, Kharkov Institute of Physics and Technology, Kharkov, Ukraine

L. Levchuk, P. Sorokin

University of Bristol, Bristol, United Kingdom

R. Aggleton, F. Ball, L. Beck, J.J. Brooke, D. Burns, E. Clement, D. Cussans, H. Flacher, J. Goldstein, M. Grimes, G.P. Heath, H.F. Heath, J. Jacob, L. Kreczko, C. Lucas, D.M. Newbold[63], S. Paramesvaran, A. Poll, T. Sakuma, S. Seif El Nasr-storey, D. Smith, V.J. Smith

Rutherford Appleton Laboratory, Didcot, United Kingdom

K.W. Bell, A. Belyaev[64], C. Brew, R.M. Brown, L. Calligaris, D. Cieri, D.J.A. Cockerill, J.A. Coughlan, K. Harder, S. Harper, E. Olaiya, D. Petyt, C.H. Shepherd-Themistocleous, A. Thea, I.R. Tomalin, T. Williams

Imperial College, London, United Kingdom

M. Baber, R. Bainbridge, O. Buchmuller, A. Bundock, D. Burton, S. Casasso, M. Citron, D. Colling, L. Corpe, P. Dauncey, G. Davies, A. De Wit, M. Della Negra, R. Di Maria, P. Dunne, A. Elwood, D. Futyan, Y. Haddad, G. Hall, G. Iles, T. James, R. Lane, C. Laner, R. Lucas[63], L. Lyons, A.-M. Magnan, S. Malik, L. Mastrolorenzo, J. Nash, A. Nikitenko[49], J. Pela, B. Penning, M. Pesaresi, D.M. Raymond, A. Richards, A. Rose, C. Seez, S. Summers, A. Tapper, K. Uchida, M. Vazquez Acosta[65], T. Virdee[16], J. Wright, S.C. Zenz

Brunel University, Uxbridge, United Kingdom

J.E. Cole, P.R. Hobson, A. Khan, P. Kyberd, D. Leslie, I.D. Reid, P. Symonds, L. Teodorescu, M. Turner

Baylor University, Waco, U.S.A.

A. Borzou, K. Call, J. Dittmann, K. Hatakeyama, H. Liu, N. Pastika

The University of Alabama, Tuscaloosa, U.S.A.

O. Charaf, S.I. Cooper, C. Henderson, P. Rumerio, C. West

Boston University, Boston, U.S.A.

D. Arcaro, A. Avetisyan, T. Bose, D. Gastler, D. Rankin, C. Richardson, J. Rohlf, L. Sulak, D. Zou

Brown University, Providence, U.S.A.

G. Benelli, E. Berry, D. Cutts, A. Garabedian, J. Hakala, U. Heintz, J.M. Hogan, O. Jesus, K.H.M. Kwok, E. Laird, G. Landsberg, Z. Mao, M. Narain, S. Piperov, S. Sagir, E. Spencer, R. Syarif

University of California, Davis, Davis, U.S.A.

R. Breedon, G. Breto, D. Burns, M. Calderon De La Barca Sanchez, S. Chauhan, M. Chertok, J. Conway, R. Conway, P.T. Cox, R. Erbacher, C. Flores, G. Funk, M. Gardner, W. Ko, R. Lander, C. Mclean, M. Mulhearn, D. Pellett, J. Pilot, S. Shalhout, J. Smith, M. Squires, D. Stolp, M. Tripathi, S. Wilbur, R. Yohay

University of California, Los Angeles, U.S.A.

C. Bravo, R. Cousins, P. Everaerts, A. Florent, J. Hauser, M. Ignatenko, N. Mccoll, D. Saltzberg, C. Schnaible, E. Takasugi, V. Valuev, M. Weber

University of California, Riverside, Riverside, U.S.A.

K. Burt, R. Clare, J. Ellison, J.W. Gary, S.M.A. Ghiasi Shirazi, G. Hanson, J. Heilman, P. Jandir, E. Kennedy, F. Lacroix, O.R. Long, M. Olmedo Negrete, M.I. Paneva, A. Shrinivas, W. Si, H. Wei, S. Wimpenny, B. R. Yates

University of California, San Diego, La Jolla, U.S.A.

J.G. Branson, G.B. Cerati, S. Cittolin, M. Derdzinski, R. Gerosa, A. Holzner, D. Klein, V. Krutelyov, J. Letts, I. Macneill, D. Olivito, S. Padhi, M. Pieri, M. Sani, V. Sharma, S. Simon, M. Tadel, A. Vartak, S. Wasserbaech[66], C. Welke, J. Wood, F. Würthwein, A. Yagil, G. Zevi Della Porta

University of California, Santa Barbara - Department of Physics, Santa Barbara, U.S.A.

N. Amin, R. Bhandari, J. Bradmiller-Feld, C. Campagnari, A. Dishaw, V. Dutta, K. Flowers, M. Franco Sevilla, P. Geffert, C. George, F. Golf, L. Gouskos, J. Gran, R. Heller, J. Incandela, S.D. Mullin, A. Ovcharova, J. Richman, D. Stuart, I. Suarez, J. Yoo

California Institute of Technology, Pasadena, U.S.A.

D. Anderson, A. Apresyan, J. Bendavid, A. Bornheim, J. Bunn, Y. Chen, J. Duarte, J.M. Lawhorn, A. Mott, H.B. Newman, C. Pena, M. Spiropulu, J.R. Vlimant, S. Xie, R.Y. Zhu

Carnegie Mellon University, Pittsburgh, U.S.A.

M.B. Andrews, V. Azzolini, T. Ferguson, M. Paulini, J. Russ, M. Sun, H. Vogel, I. Vorobiev, M. Weinberg

University of Colorado Boulder, Boulder, U.S.A.

J.P. Cumalat, W.T. Ford, F. Jensen, A. Johnson, M. Krohn, T. Mulholland, K. Stenson, S.R. Wagner

Cornell University, Ithaca, U.S.A.

J. Alexander, J. Chaves, J. Chu, S. Dittmer, K. Mcdermott, N. Mirman, G. Nicolas Kaufman, J.R. Patterson, A. Rinkevicius, A. Ryd, L. Skinnari, L. Soffi, S.M. Tan, Z. Tao, J. Thom, J. Tucker, P. Wittich, M. Zientek

Fairfield University, Fairfield, U.S.A.

D. Winn

Fermi National Accelerator Laboratory, Batavia, U.S.A.

S. Abdullin, M. Albrow, G. Apollinari, S. Banerjee, L.A.T. Bauerdick, A. Beretvas, J. Berryhill, P.C. Bhat, G. Bolla, K. Burkett, J.N. Butler, H.W.K. Cheung, F. Chlebana, S. Cihangir[†], M. Cremonesi, V.D. Elvira, I. Fisk, J. Freeman, E. Gottschalk, L. Gray, D. Green, S. Grünendahl, O. Gutsche, D. Hare, R.M. Harris, S. Hasegawa, J. Hirschauer, Z. Hu, B. Jayatilaka, S. Jindariani, M. Johnson, U. Joshi, B. Klima, B. Kreis, S. Lammel, J. Linacre, D. Lincoln, R. Lipton, T. Liu, R. Lopes De Sá, J. Lykken, K. Maeshima, N. Magini, J.M. Marraffino, S. Maruyama, D. Mason, P. McBride, P. Merkel, S. Mrenna, S. Nahn, C. Newman-Holmes[†], V. O'Dell, K. Pedro, O. Prokofyev, G. Rakness, L. Ristori, E. Sexton-Kennedy, A. Soha, W.J. Spalding, L. Spiegel, S. Stoynev, N. Strobbe, L. Taylor, S. Tkaczyk, N.V. Tran, L. Uplegger, E.W. Vaandering, C. Vernieri, M. Verzocchi, R. Vidal, M. Wang, H.A. Weber, A. Whitbeck

University of Florida, Gainesville, U.S.A.

D. Acosta, P. Avery, P. Bortignon, D. Bourilkov, A. Brinkerhoff, A. Carnes, M. Carver, D. Curry, S. Das, R.D. Field, I.K. Furic, J. Konigsberg, A. Korytov, P. Ma, K. Matchev, H. Mei, P. Milenovic[67], G. Mitselmakher, D. Rank, L. Shchutska, D. Sperka, L. Thomas, J. Wang, S. Wang, J. Yelton

Florida International University, Miami, U.S.A.

S. Linn, P. Markowitz, G. Martinez, J.L. Rodriguez

Florida State University, Tallahassee, U.S.A.

A. Ackert, J.R. Adams, T. Adams, A. Askew, S. Bein, B. Diamond, S. Hagopian, V. Hagopian, K.F. Johnson, A. Khatiwada, H. Prosper, A. Santra

Florida Institute of Technology, Melbourne, U.S.A.

M.M. Baarmand, V. Bhopatkar, S. Colafranceschi[68], M. Hohlmann, D. Noonan, T. Roy, F. Yumiceva

University of Illinois at Chicago (UIC), Chicago, U.S.A.

M.R. Adams, L. Apanasevich, D. Berry, R.R. Betts, I. Bucinskaite, R. Cavanaugh, O. Evdokimov, L. Gauthier, C.E. Gerber, D.J. Hofman, K. Jung, P. Kurt, C. O'Brien, I.D. Sandoval Gonzalez, P. Turner, N. Varelas, H. Wang, Z. Wu, M. Zakaria, J. Zhang

The University of Iowa, Iowa City, U.S.A.

B. Bilki[69], W. Clarida, K. Dilsiz, S. Durgut, R.P. Gandrajula, M. Haytmyradov, V. Khristenko, J.-P. Merlo, H. Mermerkaya[70], A. Mestvirishvili, A. Moeller, J. Nachtman, H. Ogul, Y. Onel, F. Ozok[71], A. Penzo, C. Snyder, E. Tiras, J. Wetzel, K. Yi

Johns Hopkins University, Baltimore, U.S.A.

I. Anderson, B. Blumenfeld, A. Cocoros, N. Eminizer, D. Fehling, L. Feng, A.V. Gritsan, P. Maksimovic, C. Martin, M. Osherson, J. Roskes, U. Sarica, M. Swartz, M. Xiao, Y. Xin, C. You

The University of Kansas, Lawrence, U.S.A.

A. Al-bataineh, P. Baringer, A. Bean, S. Boren, J. Bowen, C. Bruner, J. Castle, L. Forthomme, R.P. Kenny III, A. Kropivnitskaya, D. Majumder, W. Mcbrayer, M. Murray, S. Sanders, R. Stringer, J.D. Tapia Takaki, Q. Wang

Kansas State University, Manhattan, U.S.A.

A. Ivanov, K. Kaadze, S. Khalil, Y. Maravin, A. Mohammadi, L.K. Saini, N. Skhirtladze, S. Toda

Lawrence Livermore National Laboratory, Livermore, U.S.A.

F. Rebassoo, D. Wright

University of Maryland, College Park, U.S.A.

C. Anelli, A. Baden, O. Baron, A. Belloni, B. Calvert, S.C. Eno, C. Ferraioli, J.A. Gomez, N.J. Hadley, S. Jabeen, R.G. Kellogg, T. Kolberg, J. Kunkle, Y. Lu, A.C. Mignerey, F. Ricci-Tam, Y.H. Shin, A. Skuja, M.B. Tonjes, S.C. Tonwar

Massachusetts Institute of Technology, Cambridge, U.S.A.

D. Abercrombie, B. Allen, A. Apyan, R. Barbieri, A. Baty, R. Bi, K. Bierwagen, S. Brandt, W. Busza, I.A. Cali, Z. Demiragli, L. Di Matteo, G. Gomez Ceballos, M. Goncharov, D. Hsu, Y. Iiyama, G.M. Innocenti, M. Klute, D. Kovalskyi, K. Krajczar, Y.S. Lai, Y.-J. Lee, A. Levin, P.D. Luckey, B. Maier, A.C. Marini, C. Mcginn, C. Mironov, S. Narayanan, X. Niu, C. Paus, C. Roland, G. Roland, J. Salfeld-Nebgen, G.S.F. Stephans, K. Sumorok, K. Tatar, M. Varma, D. Velicanu, J. Veverka, J. Wang, T.W. Wang, B. Wyslouch, M. Yang, V. Zhukova

University of Minnesota, Minneapolis, U.S.A.

A.C. Benvenuti, R.M. Chatterjee, A. Evans, A. Finkel, A. Gude, P. Hansen, S. Kalafut, S.C. Kao, Y. Kubota, Z. Lesko, J. Mans, S. Nourbakhsh, N. Ruckstuhl, R. Rusack, N. Tambe, J. Turkewitz

University of Mississippi, Oxford, U.S.A.

J.G. Acosta, S. Oliveros

University of Nebraska-Lincoln, Lincoln, U.S.A.

E. Avdeeva, R. Bartek, K. Bloom, D.R. Claes, A. Dominguez, C. Fangmeier, R. Gonzalez Suarez, R. Kamalieddin, I. Kravchenko, A. Malta Rodrigues, F. Meier, J. Monroy, J.E. Siado, G.R. Snow, B. Stieger

State University of New York at Buffalo, Buffalo, U.S.A.

M. Alyari, J. Dolen, J. George, A. Godshalk, C. Harrington, I. Iashvili, J. Kaisen, A. Kharchilava, A. Kumar, A. Parker, S. Rappoccio, B. Roozbahani

Northeastern University, Boston, U.S.A.

G. Alverson, E. Barberis, A. Hortiangtham, A. Massironi, D.M. Morse, D. Nash, T. Orimoto, R. Teixeira De Lima, D. Trocino, R.-J. Wang, D. Wood

Northwestern University, Evanston, U.S.A.

S. Bhattacharya, K.A. Hahn, A. Kubik, A. Kumar, J.F. Low, N. Mucia, N. Odell, B. Pollack, M.H. Schmitt, K. Sung, M. Trovato, M. Velasco

University of Notre Dame, Notre Dame, U.S.A.

N. Dev, M. Hildreth, K. Hurtado Anampa, C. Jessop, D.J. Karmgard, N. Kellams, K. Lannon, N. Marinelli, F. Meng, C. Mueller, Y. Musienko[37], M. Planer, A. Reinsvold, R. Ruchti, G. Smith, S. Taroni, M. Wayne, M. Wolf, A. Woodard

The Ohio State University, Columbus, U.S.A.

J. Alimena, L. Antonelli, J. Brinson, B. Bylsma, L.S. Durkin, S. Flowers, B. Francis, A. Hart, C. Hill, R. Hughes, W. Ji, B. Liu, W. Luo, D. Puigh, B.L. Winer, H.W. Wulsin

Princeton University, Princeton, U.S.A.

S. Cooperstein, O. Driga, P. Elmer, J. Hardenbrook, P. Hebda, D. Lange, J. Luo, D. Marlow, J. Mc Donald, T. Medvedeva, K. Mei, M. Mooney, J. Olsen, C. Palmer, P. Piroué, D. Stickland, C. Tully, A. Zuranski

University of Puerto Rico, Mayaguez, U.S.A.

S. Malik

Purdue University, West Lafayette, U.S.A.

A. Barker, V.E. Barnes, S. Folgueras, L. Gutay, M.K. Jha, M. Jones, A.W. Jung, D.H. Miller, N. Neumeister, J.F. Schulte, X. Shi, J. Sun, A. Svyatkovskiy, F. Wang, W. Xie, L. Xu

Purdue University Calumet, Hammond, U.S.A.

N. Parashar, J. Stupak

Rice University, Houston, U.S.A.

A. Adair, B. Akgun, Z. Chen, K.M. Ecklund, F.J.M. Geurts, M. Guilbaud, W. Li, B. Michlin, M. Northup, B.P. Padley, R. Redjimi, J. Roberts, J. Rorie, Z. Tu, J. Zabel

University of Rochester, Rochester, U.S.A.

B. Betchart, A. Bodek, P. de Barbaro, R. Demina, Y.t. Duh, T. Ferbel, M. Galanti, A. Garcia-Bellido, J. Han, O. Hindrichs, A. Khukhunaishvili, K.H. Lo, P. Tan, M. Verzetti

Rutgers, The State University of New Jersey, Piscataway, U.S.A.

A. Agapitos, J.P. Chou, E. Contreras-Campana, Y. Gershtein, T.A. Gómez Espinosa, E. Halkiadakis, M. Heindl, D. Hidas, E. Hughes, S. Kaplan, R. Kunnawalkam Elayavalli, S. Kyriacou, A. Lath, K. Nash, H. Saka, S. Salur, S. Schnetzer, D. Sheffield, S. Somalwar, R. Stone, S. Thomas, P. Thomassen, M. Walker

University of Tennessee, Knoxville, U.S.A.

A.G. Delannoy, M. Foerster, J. Heideman, G. Riley, K. Rose, S. Spanier, K. Thapa

Texas A&M University, College Station, U.S.A.

O. Bouhali[72], A. Celik, M. Dalchenko, M. De Mattia, A. Delgado, S. Dildick, R. Eusebi, J. Gilmore, T. Huang, E. Juska, T. Kamon[73], R. Mueller, Y. Pakhotin, R. Patel, A. Perloff, L. Perniè, D. Rathjens, A. Rose, A. Safonov, A. Tatarinov, K.A. Ulmer

Texas Tech University, Lubbock, U.S.A.

N. Akchurin, C. Cowden, J. Damgov, F. De Guio, C. Dragoiu, P.R. Dudero, J. Faulkner, E. Gurpinar, S. Kunori, K. Lamichhane, S.W. Lee, T. Libeiro, T. Peltola, S. Undleeb, I. Volobouev, Z. Wang

Vanderbilt University, Nashville, U.S.A.

S. Greene, A. Gurrola, R. Janjam, W. Johns, C. Maguire, A. Melo, H. Ni, P. Sheldon, S. Tuo, J. Velkovska, Q. Xu

University of Virginia, Charlottesville, U.S.A.

M.W. Arenton, P. Barria, B. Cox, J. Goodell, R. Hirosky, A. Ledovskoy, H. Li, C. Neu, T. Sinthuprasith, X. Sun, Y. Wang, E. Wolfe, F. Xia

Wayne State University, Detroit, U.S.A.

C. Clarke, R. Harr, P.E. Karchin, J. Sturdy

University of Wisconsin - Madison, Madison, WI, U.S.A.

D.A. Belknap, C. Caillol, S. Dasu, L. Dodd, S. Duric, B. Gomber, M. Grothe, M. Herndon, A. Hervé, P. Klabbers, A. Lanaro, A. Levine, K. Long, R. Loveless, I. Ojalvo, T. Perry, G.A. Pierro, G. Polese, T. Ruggles, A. Savin, N. Smith, W.H. Smith, D. Taylor, N. Woods

†: Deceased

1: Also at Vienna University of Technology, Vienna, Austria

2: Also at State Key Laboratory of Nuclear Physics and Technology, Peking University, Beijing, China

3: Also at Institut Pluridisciplinaire Hubert Curien, Université de Strasbourg, Université de Haute Alsace Mulhouse, CNRS/IN2P3, Strasbourg, France

4: Also at Universidade Estadual de Campinas, Campinas, Brazil

5: Also at Universidade Federal de Pelotas, Pelotas, Brazil

6: Also at Université Libre de Bruxelles, Bruxelles, Belgium

7: Also at Deutsches Elektronen-Synchrotron, Hamburg, Germany

8: Also at Joint Institute for Nuclear Research, Dubna, Russia

9: Also at Suez University, Suez, Egypt

10: Now at British University in Egypt, Cairo, Egypt

11: Also at Ain Shams University, Cairo, Egypt

12: Now at Helwan University, Cairo, Egypt

13: Also at Université de Haute Alsace, Mulhouse, France

14: Also at Skobeltsyn Institute of Nuclear Physics, Lomonosov Moscow State University, Moscow, Russia

15: Also at Tbilisi State University, Tbilisi, Georgia

16: Also at CERN, European Organization for Nuclear Research, Geneva, Switzerland

17: Also at RWTH Aachen University, III. Physikalisches Institut A, Aachen, Germany

18: Also at University of Hamburg, Hamburg, Germany

19: Also at Brandenburg University of Technology, Cottbus, Germany

20: Also at Institute of Nuclear Research ATOMKI, Debrecen, Hungary

21: Also at MTA-ELTE Lendület CMS Particle and Nuclear Physics Group, Eötvös Loránd University, Budapest, Hungary

22: Also at University of Debrecen, Debrecen, Hungary

23: Also at Indian Institute of Science Education and Research, Bhopal, India

24: Also at Institute of Physics, Bhubaneswar, India

25: Also at University of Visva-Bharati, Santiniketan, India

26: Also at University of Ruhuna, Matara, Sri Lanka

27: Also at Isfahan University of Technology, Isfahan, Iran

28: Also at University of Tehran, Department of Engineering Science, Tehran, Iran

29: Also at Yazd University, Yazd, Iran

30: Also at Plasma Physics Research Center, Science and Research Branch, Islamic Azad University, Tehran, Iran

31: Also at Università degli Studi di Siena, Siena, Italy

32: Also at Purdue University, West Lafayette, U.S.A.

33: Also at International Islamic University of Malaysia, Kuala Lumpur, Malaysia

34: Also at Malaysian Nuclear Agency, MOSTI, Kajang, Malaysia

35: Also at Consejo Nacional de Ciencia y Tecnología, Mexico city, Mexico

36: Also at Warsaw University of Technology, Institute of Electronic Systems, Warsaw, Poland